© 2018. Published by The Company of Biologists Ltd | Development (2018) 145, dev168625. doi:10.1242/dev.168625

CORRECTION

Correction: Early bioelectric activities mediate redox-modulated regeneration (doi: 10.1242/dev.142034)

Fernando Ferreira, Guillaume Luxardi, Brian Reid and Min Zhao

There was an error in Development (2016) **143**, 4582-4594 (doi: 10.1242/dev.142034).

The following text was omitted from the Funding section:

This work was also supported by the Air Force Office of Scientific Research (FA9550-16-1-0052).

The authors apologise to readers for this mistake.

© 2016. Published by The Company of Biologists Ltd | Development (2016) 143, 4582-4594 doi:10.1242/dev.142034

STEM CELLS AND REGENERATION

RESEARCH ARTICLE

Early bioelectric activities mediate redox-modulated regeneration

Fernando Ferreira[1,2,*], Guillaume Luxardi[1], Brian Reid[1] and Min Zhao[1,3,*]

ABSTRACT

Reactive oxygen species (ROS) and electric currents modulate regeneration; however, the interplay between biochemical and biophysical signals during regeneration remains poorly understood. We investigate the interactions between redox and bioelectric activities during tail regeneration in *Xenopus laevis* tadpoles. We show that inhibition of NADPH oxidase-mediated production of ROS, or scavenging or blocking their diffusion into cells, impairs regeneration and consistently regulates the dynamics of membrane potential, transepithelial potential (TEP) and electric current densities (J_I) during regeneration. Depletion of ROS mimics the altered TEP and J_I observed in the non-regenerative refractory period. Short-term application of hydrogen peroxide (H_2O_2) rescues (from depleted ROS) and induces (from the refractory period) regeneration, TEP increase and J_I reversal. H_2O_2 is therefore necessary for and sufficient to induce regeneration and to regulate TEP and J_I. Epistasis assays show that voltage-gated Na^+ channels act downstream of H_2O_2 to modulate regeneration. Altogether, these results suggest a novel mechanism for regeneration via redox-bioelectric orchestration.

KEY WORDS: NADPH oxidases, Reactive oxygen species, Membrane potential, Transepithelial potential, Electric current density, Voltage-gated Na^+ channels, Regeneration, *Xenopus laevis*

INTRODUCTION

Understanding large-scale repair via regeneration is a fundamental issue in basic biology and regenerative medicine. Biochemical signals, such as Wnt and BMP pathways, have been extensively studied and have been shown to control regeneration (Alvarado and Tsonis, 2006; Stoick-Cooper et al., 2007). Reactive oxygen species (ROS), especially hydrogen peroxide (H_2O_2), are suggested to act as signaling cues in the wound microenvironment (Sen and Roy, 2008; Veal et al., 2007). Upon wounding, the *Drosophila* embryo (Moreira et al., 2010), zebrafish larva (Niethammer et al., 2009) and *Xenopus* tadpole (Love et al., 2013) produce a H_2O_2 gradient that precedes the oxidative burst. This gradient, in fact, attracts immune cells toward the wound edges. In addition, a redox sensor has been identified in the leading edge of neutrophils (Wittmann et al., 2012; Yoo et al., 2011, 2012) and topical application of low doses of H_2O_2 enhances wound closure in mice (Loo et al., 2012). Importantly, ROS are required for the regeneration of planarian head and tail (Pirotte et al., 2015), zebrafish caudal fin (Gauron et al., 2013) and heart (Han et al., 2014), *Xenopus* tadpole tail (Love et al., 2013), and gecko tail (Zhang et al., 2016).

In addition to ROS, biophysical signals such as the dynamic bioelectric activities measured during regeneration have been proposed to act as signaling cues (Levin, 2007; McCaig et al., 2005). It has been shown that transepithelial potential (TEP)-driven electric current densities (J_I) correlate with and are required for regeneration in amphibians (Borgens et al., 1977b; Jenkins et al., 1996; Nawata, 2001; Reid et al., 2009). Electrical stimulation induces some regeneration in non-permissive adult frog and rat limbs (Becker, 1972; Borgens et al., 1977a; Leppik et al., 2015; Smith, 1967). Moreover, engineered devices (Golding et al., 2016) partially induce mouse digit tip regeneration (Hechavarria et al., 2010) and are in clinical trials to improve paraplegia (Shapiro et al., 2005). Re-emerging bioelectric studies are revealing transduction mechanisms. V-ATPase-mediated repolarization of membrane potential (V_m) and voltage-gated Na^+ channel (VGSC or Na_V) 1.2-mediated sodium influx are necessary for and sufficient to induce *X. laevis* tadpole tail regeneration (Adams et al., 2007; Tseng et al., 2010). V-ATPase proton efflux activity correlates with regeneration rate and ability in zebrafish caudal fin regeneration (Monteiro et al., 2014). H^+/K^+-ATPase-mediated V_m depolarization modulates planarian head regeneration (Beane et al., 2011). In addition, ion and V_m dynamics correlate with axolotl larvae tail regeneration (Özkucur et al., 2010).

Interestingly, redox and bioelectric activities control the expression and activity of signaling pathways, such as Wnt, FGF, BMP and Notch, in addition to cell behaviors, such as proliferation, apoptosis and innervation, which are required for regeneration (Adams et al., 2007; Gauron et al., 2013; Han et al., 2014; Love et al., 2013; Monteiro et al., 2014; Tseng et al., 2010). Redox (ROS) and bioelectric [V_m, TEP, electric fields (EF) and J_I] states therefore affect regeneration. But how do these signals integrate? Do they act in parallel or in series during regeneration? *Xenopus laevis* tadpole tail regeneration provides an ideal model with which to address these questions (Love et al., 2013; Reid et al., 2009). The tail comprises epidermis, muscle, blood vessels and spinal cord, making it a prime model for biomedical research (Beck et al., 2009; Deuchar, 1975). In addition, the fluctuating regenerative abilities of tails through developmental stages offer unique opportunities to study regeneration-deficient tails, in the refractory period (Beck et al., 2003), using the same model organism.

RESULTS

Do ROS modulate regeneration via the regulation of V_m, TEP, EF and/or J_I, all of which are known to be required for regeneration? At the cellular level, NADPH oxidases in the cell membrane catalyze electron transfer from cytoplasmic NADPH to extracellular molecular O_2, generating ROS and depolarizing V_m (Demaurex and Petheö, 2005; Lambeth and Neish, 2014). This dual property – electrogenic and catalytic – of NADPH oxidases led us to hypothesize a two-way regulation: (1) the activity of NADPH

[1]Department of Dermatology, Institute for Regenerative Cures, University of California, Davis, CA 95817, USA. [2]Departamento de Biologia, Centro de Biologia Molecular e Ambiental (CBMA), Universidade do Minho, Braga 4710, Portugal. [3]Department of Ophthalmology, Institute for Regenerative Cures, University of California, Davis, CA 95817, USA.

*Authors for correspondence (fdasilvaferreira@ucdavis.edu; minzhao@ucdavis.edu)

M.Z., 0000-0002-2500-3035

Received 9 July 2016; Accepted 21 October 2016

Development (2016) 143, 4582-4594 doi:10.1242/dev.142034

oxidases per se depolarizes V_m; and (2) the ROS produced, especially H_2O_2, regulate TEP, EF and J_I. To test this hypothesis, we performed descriptive spatiotemporal profiling and functional assays.

Injury-induced extracellular bioelectricity dynamically correlates with regeneration

We first mapped the extracellular bioelectricity, TEP, EF and J_I, during regeneration to select key spatiotemporal points at which to test the two-way regulation hypothesis. Regeneration can be divided into three phases, structurally completed in 7 days (Beck et al., 2009; Tseng et al., 2010): (1) wound healing [until ∼6 h post-amputation (hpa)] – wound epithelium covers amputation plane; (2) regeneration bud formation (∼24 hpa) – bud produces progenitor cells; and (3) regenerative outgrowth (∼48 hpa and after) – outgrowth and patterning reestablishes tail structure and function (Fig. 1A, Fig. S5).

Before amputation, baseline trunk TEP was 28.64±2.27 mV (inside positive; n=9) and the tail tip had small inward currents of −0.04±0.005 µA cm^{-2} (n=7) (Fig. 1B, Fig. S2C). EF were assumed to be 0 mV mm^{-1}, because over the measured distances (<1 mm), no consistent TEP gradients were detected. Upon amputation, a TEP short-circuit (to 0 mV) at the stump generated a strong lateral $EF_{Trunk\rightarrow Bud}$ of −85.50 mV mm^{-1} (calculated using uncut TEP) and a low-resistance pathway leaking outward currents (the injury current) of 13.27±2.807 µA cm^{-2} (at 0.08 hpa; n=6, P=0.005) in the bud (Fig. 1B-D). Spatial profiles showed a consistent anteroposterior (A/P) gradient either directly (for TEP) or inversely (for EF) proportional to the distance from the amputation plane and evolving circuits (for J_I and EF) during regeneration (Figs S2-S5). The spatial profile of J_I was intended to unveil circuit loops (primarily dorsoventral) more than gradients (cases of TEP and V_m).

Temporal profiles presented exponential-like curves, positive for TEP recovery and for EF (Fig. 1B,C), and negative for J_I (Fig. 1D), that correlated with regeneration. The dramatic TEP recovery (to 67.42±5.35%, n=26, P<0.0001 versus 1 hpa), decrease in EF (to −22.94±4.89 mV mm^{-1}, n=23, P=0.0002 versus 1 hpa; 73% drop versus 0.08 hpa) and J_I reversal (to −0.10±0.017 µA cm^{-2}, n=27, P=0.005 versus 0.08 hpa; 99% shift) by 6 hpa (Fig. 1B-D) match the wound epithelium formation phase and possible bud initiation (Fig. 1A,E, Fig. S5). Spatially, J_I reversals progressed in a centripetal way until 6 hpa, lastly in the bud (Fig. S4C), which is possibly due to centripetal healing. We descriptively termed this part of the curve as 'slope' ('S'; Fig. 1B-D). Analogous TEP recovery is seen in wound healing assays *in vitro* (human skin) and *in vivo* (porcine skin) (Dubé et al., 2010). Similar drops in EF (75%) and J_I reversal (in the spinal cord) by 6 hpa occur in newt limbs and *X. laevis* tadpole tail regeneration, respectively (McGinnis and Vanable, 1986; Reid et al., 2009). From 6 to 48 (especially to 24) hpa, TEP, EF and J_I stabilization (P≫0.05 to all comparisons from 6 to 24 hpa; Fig. 1B-D) correlated with the regeneration bud formation phase (Fig. 1A,E, Fig. S5). We termed this part of the curve as 'plateau' ('P'; Fig. 1B-D). From 48 hpa onwards, a final shift completed TEP recovery (Fig. 1B; bud versus trunk non-significant at 72 hpa, n=11, P=0.106; Fig. S2C), resolved EF (−10.74± 7.12 mV mm^{-1} at 72 hpa, n=11; Fig. 1C) and returned J_I to even lower than uncut baseline (−0.01±0.002 µA cm^{-2} at 48 hpa, n=11, P<0.0001; Fig. 1D). The very small J_I from 48 hpa might be due to the increased surface area to volume ratio, which is due to the animal growth. We therefore termed this part of the curve as 'baseline' ('B'; Fig. 1B-D) and it correlated with regenerative outgrowth phase (Fig. 1A,E, Fig. S5). Altogether, extracellular bioelectricity shows a dynamic correlation with regeneration and suggests that the bud at 6 hpa is a key spatiotemporal point to test the proposed hypothesis.

Injury-induced ROS production, availability and diffusion are necessary for regeneration

Next, we sought to clarify whether H_2O_2 is the main ROS involved in regeneration. We used drugs that target specific steps of the ROS 'life cycle' (see Fig. 6A): (1) production – by blocking NADPH oxidases with diphenyleneiodonium (DPI) (O'Donnell et al., 1993); (2) availability – by scavenging ROS with MCI-186 (MCI) (Otomo, 2003); and (3) diffusion – by preventing entry of H_2O_2 into cells through aquaporins with $AgNO_3$ (Niemietz and Tyerman, 2002). As previously shown (Han et al., 2014; Love et al., 2013; Niethammer et al., 2009), we confirmed that these drugs decreased levels of intracellular ROS in the bud (Fig. S6).

Similarly to another study (Love et al., 2013), DPI-treated tadpoles showed significantly inhibited regeneration, with virtually all tails presenting either a weak (35%, sixfold increase relative to vehicle control 6%) or none (64%, >50-fold increase) phenotype [regeneration index (RI) reduced from 255, n=233, to 39, n=74, P<0.0001; Fig. 2A,A′]. To establish NADPH oxidases as the main ROS source for regeneration, we used the alternative drugs apocynin (Simons et al., 1990) and VAS2870 (VAS) (ten Freyhaus et al., 2006). Besides being less penetrant than DPI, both drugs significantly impaired regeneration (Fig. S7A). Scavenging ROS with the antioxidant MCI significantly impaired regeneration with a 83% decrease in full (11%) and a fourfold increase in weak (24%) phenotypes (RI reduced from 255 to 187, n=43, P=0.005; Fig. 2A,A′). More penetrant effects of MCI have previously been shown if quantified at 3 days post-amputation (dpa), but not at 7 dpa (Love et al., 2013). Most H_2O_2 diffuses through aquaporins, such as AQP3 and AQP8 (Bienert and Chaumont, 2014; Miller et al., 2010). Highly specific small-molecule drugs for aquaporins are not yet available (Verkman et al., 2014) so we used $AgNO_3$. $AgNO_3$-treated tadpoles showed significantly impaired regeneration with a 69% reduction in the full phenotype (20%), and four- and fivefold increases in, respectively, the weak (25%) and the none (7%) phenotypes (RI reduced from 255 to 182, n=65, P<0.0001; Fig. 2A,A′). Penetrance on regeneration inhibition was therefore DPI≫$AgNO_3$>MCI (Fig. 2A′). Altogether, H_2O_2 is probably the main ROS responsible for the impaired regeneration and it must diffuse into cells, likely via aquaporins, to be effective.

Love et al. have shown that ROS production for the first 3 days is enough to impair regeneration (Love et al., 2013). We tested the role for ROS earlier, in wound epithelium and regeneration bud form, because both are limiting factors of regeneration (Fig. S7B-C′). We started by testing DPI until 6 and 24 hpa. These experiments still robustly inhibited regeneration (until 6 hpa, RI reduced from 246, n=94, to 160, n=52, P<0.0001; until 24 hpa, RI reduced to 89, n=50, P<0.0001; Fig. S7B). VAS treatment confirmed this early requirement (Fig. S7A). Next, we extended the temporal screening and found that ROS are also necessary for the last phase of regeneration (48 hpa onwards), although not for morphogenesis (RI) but for growth (area) (Fig. S7B-B″). This is congruent with impaired proliferation produced by inhibition of NADPH oxidases (Gauron et al., 2013; Han et al., 2014; Love et al., 2013). Finally, by increasing DPI dose, we found that ROS are immediately necessary for regeneration (Fig. S7C,C′). Altogether, ROS presented multi-

Development (2016) 143, 4582-4594 doi:10.1242/dev.142034

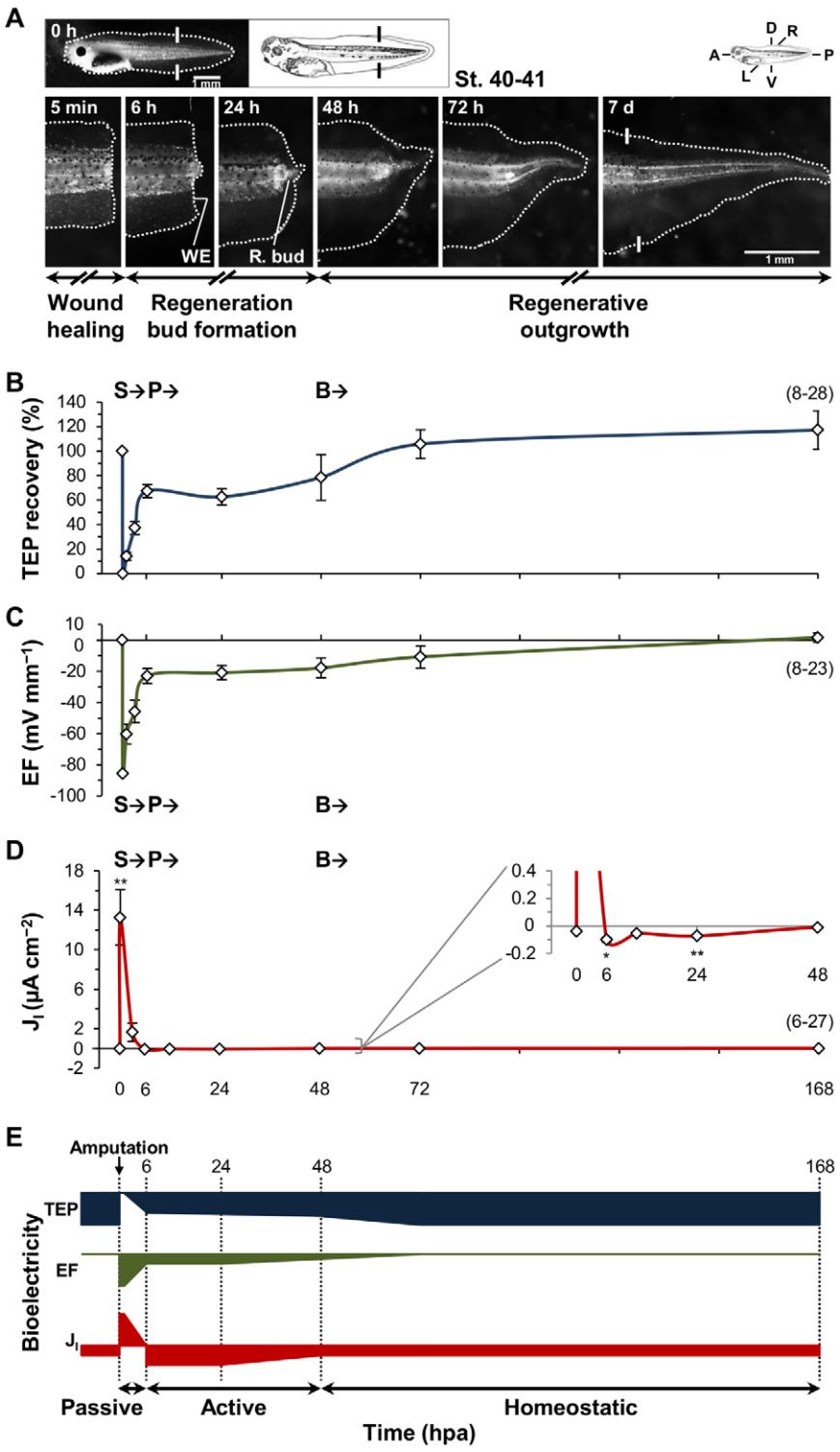

Fig. 1. Extracellular bioelectricity dynamically correlates with regeneration. (A) Regeneration time-lapse and phases of a representative tadpole tail amputated at stage 40-41. Major phenotypic structures annotated: wound epithelium (WE) and regeneration bud (R. bud). Photomicrographs of regenerating or regenerated tails are displayed in the same orientation as the whole organism showing anteroposterior (A/P), dorsoventral (D/V) and left-right (L/R) axes (top left scheme; applies to subsequent figures). White solid lines: amputation plane (black solid lines in schematic tadpole). Scale bars: 1 mm. (B) Temporal profile of TEP recovery in the regeneration bud in vehicle control (DMSO 0.1%). Calculated from data in Fig. S2C. (C) Temporal profile of lateral, trunk to bud, EF in vehicle control. Calculated from data in Fig. S2C. (D) Temporal profile of J_I in the bud in vehicle control. Conventional current flow is used, thus positive values are net outward and negative are net inward currents (applies to subsequent figures). Profiles B-D are descriptively divided into three parts: S, slope; P, plateau; and B, baseline. (E) Diagrammatic representation integrating the temporal dynamics of TEP recovery, $EF_{Trunk \rightarrow Bud}$ and J_I during regeneration. Profiles are divided into three phases according to the bioelectric activity: passive, active and homeostatic. Magnitudes are not absolute but present the relative dynamics in temporal directions and magnitudes. Same *x*-axis labels for B-D; same *x*-axis titles for B-E. For B-D, *n* specimens indicated in brackets.

phase pleiotropic effects during regeneration and NADPH oxidase-mediated ROS production is, to our knowledge, potentially the earliest biochemical limiting factor of regeneration.

NADPH oxidase-driven electron flow depolarizes V_m in the regeneration bud at 6 hpa

Cellular bioelectricity has previously been characterized in the same *X. laevis* model (Adams et al., 2007) and in axolotl larvae (Özkucur et al., 2010). These studies showed a robust V_m depolarization in the bud at 6 hpa that should repolarize by 24 hpa for complete regeneration (Adams et al., 2007). However, the origin of depolarization is unknown. V_m depolarization (Adams et al., 2007) and H_2O_2 concentration (Love et al., 2013) appear to overlap spatiotemporally. Activity of NADPH oxidases generates an electron flow that depolarizes V_m in immune cells that can be used as a direct quantification of holoenzyme activity (Demaurex and Petheö, 2005).

Development (2016) 143, 4582-4594 doi:10.1242/dev.142034

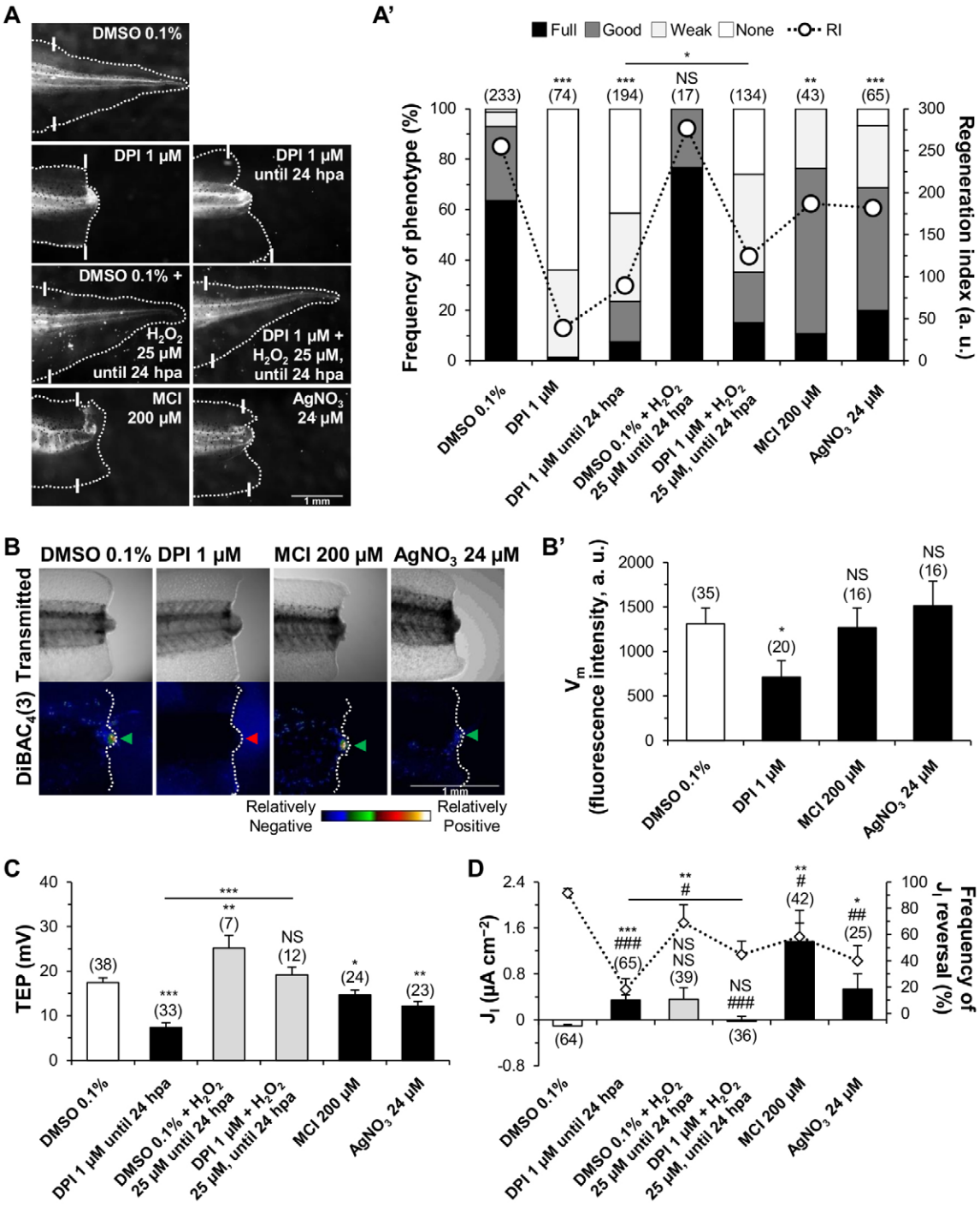

Fig. 2. Electrogenic property of NADPH oxidases is necessary for V_m depolarization and catalytic property for regeneration, TEP increase and J_I reversal. (A,A′) Loss and rescue of regeneration by ROS and H_2O_2 modulation. (A) Representative 7 dpa tails from vehicle-control (DMSO 0.1%) and pharmacologically treated tadpoles. White lines: amputation plane. (A′) Qualitative and quantitative analyses of regeneration efficiency for the different conditions tested. RI, regeneration index. (B,B′) Activity of NADPH oxidases per se depolarizes V_m. (B) Representative tails under transmitted light (top panels) and fluorescence imaging (bottom panels) of membrane potential-sensitive dye $DiBAC_4(3)$ in vehicle control and after pharmacological treatment at 6 hpa. Green arrowhead, V_m depolarization (relatively positive) in the bud; red arrowhead, no V_m depolarization in the bud. (B′) Semi-quantitative analysis of V_m for the different conditions tested. (C,D) Pharmacological loss and rescue of regeneration are correlated with variations of TEP (C) and J_I (D). In D, frequencies of current reversals (mean percentage of inward J_I, diamonds) also correlated with pharmacological treatment. *P<0.05 versus J_I magnitude; #P<0.05 versus J_I reversals; **,##P<0.01; ***,###P<0.001. a.u., arbitrary units. Scale bars: 1 mm; *n* values are indicated in brackets.

To test whether the activity of NADPH oxidases induced the V_m depolarization, we blocked them with DPI and imaged V_m with the membrane potential-sensitive dye $DiBAC_4(3)$ (Fig. S8A). DPI-treated tails at 6 hpa were, as in vehicle controls, still depolarized in the bud in relation to the rest of the tail (bud≫shoulder>trunk; Fig. S8A′), but had a significantly decreased depolarization (46% reduction, n=20, P=0.033; Fig. 2B,B′). Consequently, the spatial A/P gradient was also reduced (Fig. S8A′).

Development (2016) 143, 4582-4594 doi:10.1242/dev.142034

To exclude a possible effect of ROS/H_2O_2 in V_m, we next scavenged and prevented them from diffusing into cells as before. MCI- and $AgNO_3$-treated tails showed no V_m variation in the bud at 6 hpa (n=16, P>0.05 to both; Fig. 2B,B′). Therefore, V_m depolarization in the bud at 6 hpa is originated by the activity of NADPH oxidases per se.

H_2O_2 regulates TEP increase and J_I reversal in the regeneration bud

Next, we tested whether H_2O_2 regulates TEP, EF and J_I. To achieve this, we blocked ROS/H_2O_2 production, availability and diffusion as before and measured TEP and J_I in the bud at 6 hpa. DPI-treated tails showed a significantly decreased TEP (58% reduction, from 17.42±1.11, n=38, to 7.33±1.08 mV, n=33, P<0.0001; Fig. 2C). DPI reversed the direction of some TEPs to negative inside (e.g. 12% of total at 6 hpa). MCI- and $AgNO_3$-treated tadpoles also had significantly decreased TEPs (MCI, 16% reduction, n=24, P=0.046; $AgNO_3$, 30% reduction, n=23, P=0.002; Fig. 2C).

Drug-treated shoulder and trunk (amputated or uncut) TEP shifted in the same way as bud TEP (Figs S8B, S12C,D), suggesting a systemic baseline shift and effect on housekeeping translocators. As a consequence, spatial A/P gradients remained relatively unaffected (Fig. S8B), leading to constant TEP recoveries and long-range $EF_{Trunk\rightarrow Bud}$ (Fig. S12E). However, short-range $EF_{Shoulder\rightarrow Bud}$ presented increased magnitudes (Fig. S16A), potentially powered by J_I direction (below). For these reasons, we mainly compared absolute TEP in bud.

The TEP decrease, caused by depleted H_2O_2, anticipated an effect of H_2O_2 on J_I. Almost all (91.60±3.38%) vehicle-control bud currents reversed at 6 hpa, giving a net inward J_I (−0.10± 0.025 μA cm^{-2}, n=64). Only 18.05± 8.32% reversed in DPI-treated tadpoles, maintaining a significant outward J_I (0.34± 0.096 μA cm^{-2}, n=65, P<0.0001; Fig. 2D). Indeed, steady outward J_I were measured for days (Fig. S9A). Further analysis showed the reversibility of DPI-prevented reversal (Fig. S9B). MCI and $AgNO_3$ treatments also prevented reversal at 6 hpa with significant outward J_I (MCI, n=42, P<0.01, 58.33± 10.41% reversal; $AgNO_3$, n=25, P=0.026, 40.00±11.55% reversal; Fig. 2D). Unlike DPI, J_I in MCI- and $AgNO_3$-treated tails reversed by 24 hpa (Fig. S8C), mimicking the refractory period (Fig. S11C).

Spatially, drug-sustained outward current at 6 hpa precluded an evolving electrical circuit (Figs S8C, S9C) and probably contributed to maintaining EF direction (cathode in the bud) and to increasing EF magnitude (Fig. S16A). Importantly, the penetrance of the drugs on TEP decrease and J_I reversal was equal to impaired regeneration (DPI≫$AgNO_3$>MCI; Fig. 2A′,C,D). Altogether, the TEP increase and J_I reversal are regulated by H_2O_2 that diffuses into cells, likely via aquaporins.

Exogenous H_2O_2 rescues regeneration, TEP increase and J_I reversal

After demonstrating that H_2O_2 is required for regeneration and regulates TEP and J_I, we performed stimulation assays. We first attempted to rescue DPI-impaired regeneration, TEP and J_I using exogenous H_2O_2. To impose a suitable spatiotemporal redox state was challenging due to diverse cell responses (physiological and biochemical) to disparate ROS levels. Briefly, high levels might produce oxidative stress, whereas low levels produce more signaling effects (Lambeth and Neish, 2014). Long-term exposure to H_2O_2 could turn counterproductive by setting too much of a steady state in the very dynamic process of regeneration. In addition, regeneration-specific events are more likely to be present within 24 hpa. Therefore, we focused on application of H_2O_2 in low doses (μM range) and for a short exposure (first 24 h).

H_2O_2 until 24 hpa significantly rescued DPI-impaired regeneration, TEP increase and J_I reversal (Fig. 2A,A′,C,D). H_2O_2 increased twofold the frequency of full phenotypes compared with DPI-treated tails (from 7 to 15%) and decreased 37% the frequency of none phenotypes (from 41 to 26%). Overall, regeneration was significantly rescued (RI from 90, n=194, to 124, n=134, P=0.016; Fig. 2A,A′). Long-term (7 days) exposure to H_2O_2 did not rescue regeneration (Fig. S13), pointing to the importance of redox state dynamics (Loo et al., 2012).

TEP magnitude in the bud at 6 hpa was entirely rescued to values slightly higher than vehicle control [dimethyl sulfoxide (DMSO): 17.42±1.11 mV, n=38; DPI+H_2O_2: 19.15±1.72 mV, n=12; P=0.435; Fig. 2C]. H_2O_2 significantly rescued 161% of TEP (from 7.33±1.08, n=33, to 19.15±1.72 mV, n=12, P<0.0001; Fig. 2C) and enhanced 45% of TEP (from 17.42±1.11 to 25.20± 2.84 mV, n=7, P=0.009; Fig. 2C). As for DPI, MCI and $AgNO_3$, shoulder and trunk (amputated or uncut) TEP shifted in the same way as bud TEP (Figs S8B, S12C-E).

J_I magnitude and J_I reversal in the bud at 6 hpa were dramatically rescued to values closer to vehicle control (DMSO: −0.10± 0.025 μA cm^{-2}, 91.60±3.38% reversal, n=64; DPI+H_2O_2: −0.02± 0.086 μA cm^{-2}, 44.76±10.05% reversal, n=36; P=0.395; Fig. 2D). H_2O_2 significantly rescued 105% of J_I magnitude to inward current (from 0.34±0.096, n=65, to −0.02± 0.086 μA cm^{-2}, n=36, P=0.005; Fig. 2D). Importantly, current reversals more than doubled (from 18.05±8.32 to 44.76±10.05%, P=0.029; Fig. 2D). Unlike the changes induced in TEP, H_2O_2 neither enhanced J_I magnitude nor J_I reversal frequency in vehicle control. Nonetheless, most currents still reversed by 6 hpa (69.05± 13.52%), resulting in a large variance (0.36±0.204 μA cm^{-2}, n=39, P=0.114; Fig. 2D). Altogether, short-term exposure to low-dose H_2O_2 rescued DPI-impaired regeneration, TEP increase and J_I reversal. In addition, these results suggest that the electrogenicity of NADPH oxidases may not affect TEP and J_I.

Exogenous H_2O_2 induces regeneration, TEP increase and J_I reversal in the refractory period

The *X. laevis* non-regenerative refractory period provides a unique advantage among regeneration models. We explored it to test whether we could induce regeneration, TEP and J_I using exogenous H_2O_2. First, we verified whether the refractory period has impaired bioelectricity. Remarkably, TEP decrease and postponed J_I reversal in the bud mimicked the effects of depleted ROS (Fig. S11). Blocked J_I reversal has previously been shown in the spinal cord (Reid et al., 2009). Application of H_2O_2 until 24 hpa increased the frequency of full phenotypes by 2.4-fold (from 13 to 31%) and decreased the frequency of none phenotypes by 62% (from 39 to 15%). Overall, regeneration was significantly induced (RI from 110, n=55, to 174, n=51, P=0.004; Fig. 3A,A′). As for rescue, long-term (7 days) exposure to H_2O_2 did not induce regeneration (Fig. S13).

The magnitude of the TEP in the bud at 6 hpa increased to values slightly higher than those found during the regenerative period (DMSO stage 40-41: 23.10±1.74 mV, n=14; DMSO stage 45-46+ H_2O_2: 25.92±1.54 mV, n=18; P=0.235; Fig. 3B). H_2O_2 raised the TEP by 115% (from 12.04±1.45, n=14, to 25.92±1.54 mV, n=18, P<0.0001; Fig. 3B). In addition, H_2O_2 shoulder and trunk (amputated or uncut) TEP shifted in the same way as bud TEP (Figs S10A and S12C-E).

J_I magnitude and J_I reversal in the bud at 6 hpa were dramatically induced to values closer to those found during the regenerative

Development (2016) 143, 4582-4594 doi:10.1242/dev.142034

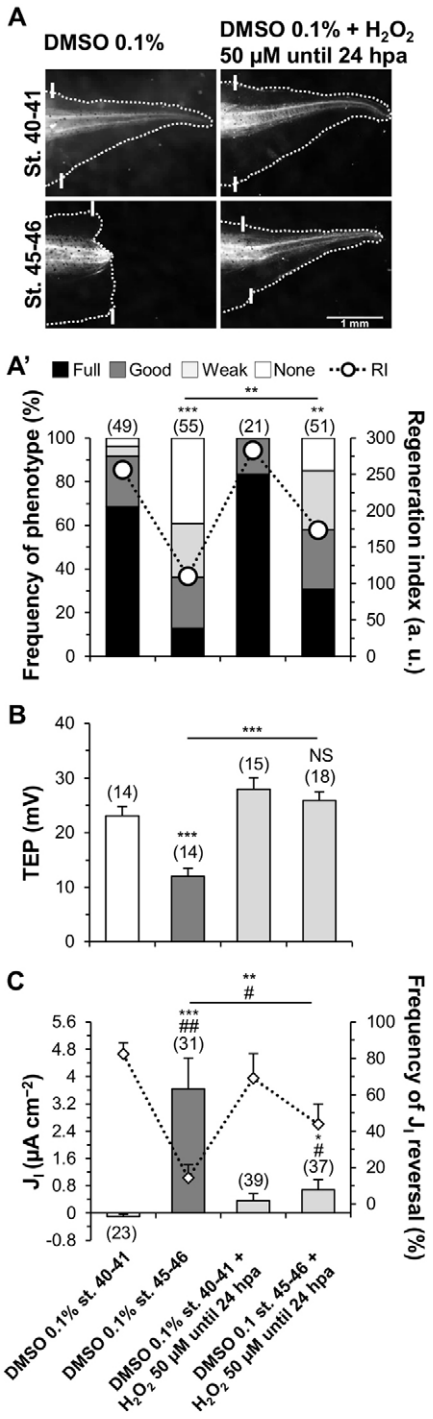

Fig. 3. Exogenous H_2O_2 is sufficient to induce regeneration, TEP increase and J_I reversal during the refractory period. (A,A′) Induction of regeneration by exogenous H_2O_2. (A) Representative 7 dpa tails from tadpoles amputated during the regenerative (stage 40-41) or refractory period (stage 45-46). Vehicle-control (DMSO 0.1%) and H_2O_2-treated (50 µM until 24 hpa) results are shown. White solid lines, amputation plane. Scale bar: 1 mm. (A′) Qualitative and quantitative analyses of regeneration efficiency for the different conditions tested. RI, regeneration index; a.u., arbitrary units. (B,C) Exogenous H_2O_2-mediated induction of regeneration is correlated with variations of TEP (B) and J_I (C). In C, frequencies of current reversals (mean percentage of inward J_I, diamonds) also correlated with pharmacological treatment. *P<0.05 versus J_I magnitude; #P<0.05 versus J_I reversals; **,##P<0.01; ***,###P<0.001. Horizontal axis labels in C also apply to A′,B. n values are indicated in brackets.

period (DMSO stage 40-41: −0.10±0.065 µA cm^{-2}, 82.34±6.27% reversal, n=23; DMSO stage 45-46+H_2O_2: 0.68±0.296 µA cm^{-2}, 43.81±11.18% reversal, n=37; P=0.013; Fig. 3C, Fig. S10B). H_2O_2 significantly decrease J_I magnitude in 81% to a still outward current (from 3.64±0.897, n=31, to 0.68±0.296 µA cm^{-2}, n=37, P=0.003; Fig. 3C). Importantly, current reversals increased threefold (from 14.29±7.19 to 43.81±11.18%, P=0.044; Fig. 3C).

We then attempted to induce ectopic tail formation during the regenerative period. Upon dorsal incisions, H_2O_2 treatment for 24 h slightly induced significant ectopic (abnormal or complete) tail formation (up to a frequency of 19%) in a dose-independent way (Fig. S15). Altogether, short-term exposure to low-dose H_2O_2 is sufficient to induce regeneration, TEP increase and J_I reversal during the refractory period, in addition to inducing ectopic tail formation in the regenerative period.

Regeneration efficiency correlates linearly with TEP magnitude and J_I reversals

Following the parallel responses of regeneration, TEP and J_I to the different conditions used, we tested whether bioelectricity predicts regeneration efficiency. Plotting all conditions together showed a significant linear correlation of regeneration efficiency with TEP magnitude (r=0.74, P=0.036; Fig. S14) and with the frequency of J_I reversals (r=0.86, P=0.006; Fig. 4).

Voltage-gated Na^+ channels are required for H_2O_2-modulated regeneration

To unveil the mechanisms by which H_2O_2 modulates regeneration, we searched for ion translocators that ideally affect regeneration and bioelectricity. $Na_V1.2$ is required for *X. laevis* tadpole tail regeneration via Na^+ influx control (Tseng et al., 2010). Therefore, we tested whether Na_V channels act downstream of H_2O_2 using complementary epistasis assays. First, we verified that the inhibition of Na_V channels impairs regeneration. As expected (Tseng et al., 2010), the Na_V inhibitor tricaine (Frazier and

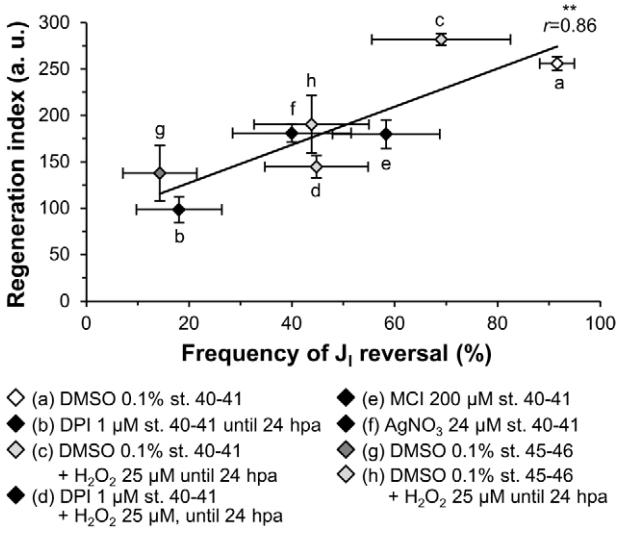

Fig. 4. Regeneration efficiency is directly proportional to J_I reversals. Compilation of the different conditions tested. Data of regeneration index are from Figs 2A′, 3A′ and data of frequency of J_I reversal are from Figs 2D, 3C. Most crossed data are matched siblings. Solid line, linear regression (r^2=0.75); r, correlation coefficient.

Development (2016) 143, 4582-4594 doi:10.1242/dev.142034

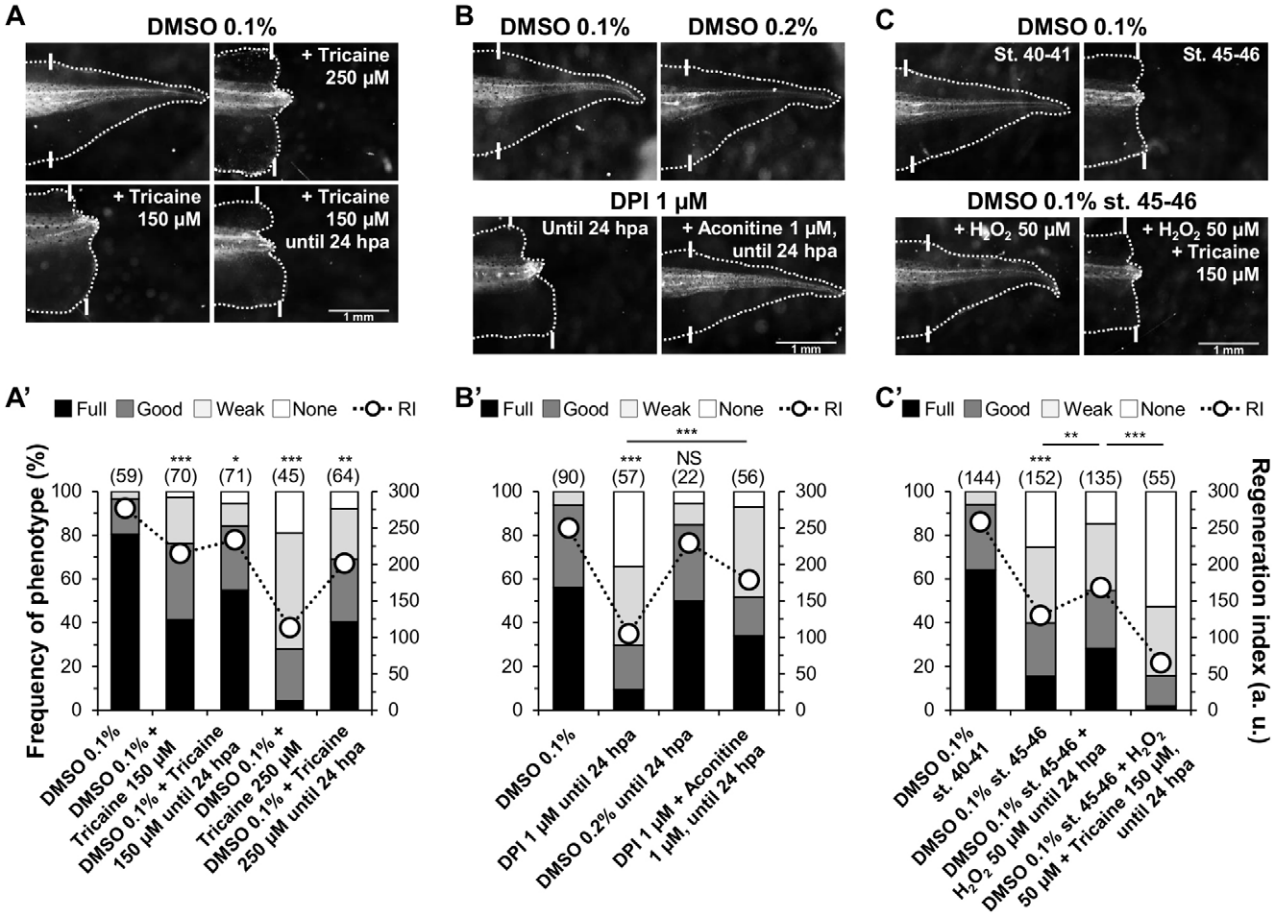

Fig. 5. H_2O_2 modulates regeneration via voltage-gated Na^+ (Na_V) channels. (A,A′) Na_V channel inhibition with tricaine impaired regeneration. (A) Representative 7 dpa tails treated with vehicle (DMSO 0.1%) or tricaine (250 or 150 µM) from amputation or until 24 hpa. (A′) Qualitative and quantitative analyses of regeneration efficiency for the different conditions tested. (B,B′) Na_V channel activation with aconitine rescued DPI-impaired regeneration. (B) Representative 7 dpa tails treated with vehicle (DMSO 0.1% and DMSO 0.2%) or DPI (1 µM), alone or with aconitine (1 µM), until 24 hpa. (B′) Qualitative and quantitative analyses of regeneration efficiency for the different conditions tested. (C,C′) Na_V channel inhibition abolished H_2O_2-induced regeneration in the refractory period. (C) Representative 7 dpa tails amputated from tadpoles during the regenerative (stage 40-41) or refractory (stage 45-46) periods. Tails were treated until 24 hpa with vehicle, with H_2O_2 (50 µM) alone, or with H_2O_2 (50 µM) plus tricaine (150 µM). (C′) Qualitative and quantitative analyses of regeneration efficiency for the different conditions tested. Primary vertical axis title in A′ also applies to B′,C′; secondary vertical axis title in C′ also applies to A′,B′. RI, regeneration index; a.u., arbitrary units. White solid lines, amputation plane. Scale bars, 1 mm; *n* values are indicated in brackets.

Narahashi, 1975) significantly impaired regeneration (250 µM: RI reduced from 277, n=59, to 113, n=45, P<0.0001; 250 µM until 24 hpa: RI reduced to 202, n=64, P=0.008). A lower dose (150 µM) had less penetrant effects (Fig. 5A,A′). Next, we designed the epistasis assays: (1) rescue DPI-impaired regeneration using the Na_V activator aconitine; and (2) loss H_2O_2-induced regeneration in the refractory period using the Na_V inhibitor tricaine.

Treatment with aconitine (Ameri, 1998) until 24 hpa significantly rescued DPI-impaired regeneration (Fig. 5B,B′). Aconitine increased 3.6-fold the frequency of tails with full phenotypes in relation to DPI-treated tails (from 9 to 34%) and decreased by ~80% the frequency of none phenotypes (from 34 to 7%). Overall, regeneration was significantly rescued (RI from 105, n=57, to 179, n=56, P<0.0001; Fig. 5B,B′). Interestingly, aconitine (in the µM range) was lethal in the absence of DPI, pointing to antagonistic competition.

Treatment with tricaine until 24 hpa significantly impaired H_2O_2-induced regeneration (Fig. 5C,C′). Tricaine virtually eliminated full phenotypes in relation to H_2O_2-treated tails (from 30 to 2%) and increased 3.4-fold the frequency of none phenotypes (from 17 to 57%). Overall, regeneration was significantly lost (RI from 168, n=135, to 65, n=55, P<0.0001; Fig. 5C,C′). Therefore, Na_V channels act downstream of H_2O_2 and mediate H_2O_2-modulated regeneration – a new mechanism.

DISCUSSION

Bioelectric and, more recently, redox activities have been shown, independently, to modulate regeneration in widespread models: planaria (Beane et al., 2011; Pirotte et al., 2015), zebrafish (Gauron et al., 2013; Monteiro et al., 2014) and amphibians (Love et al., 2013; Reid et al., 2009). Seeking a biochemical and biophysical integration, we aimed to determine whether and how these pervasive activities interact during regeneration.

Redox-modulated regeneration is mediated by early bioelectric activities

Do ROS modulate regeneration via regulation of bioelectric activities that are known to be required for regeneration? Our results support the two-way regulation hypothesis proposed to address this question. First we mapped the spatiotemporal dynamics of extracellular

Development (2016) 143, 4582-4594 doi:10.1242/dev.142034

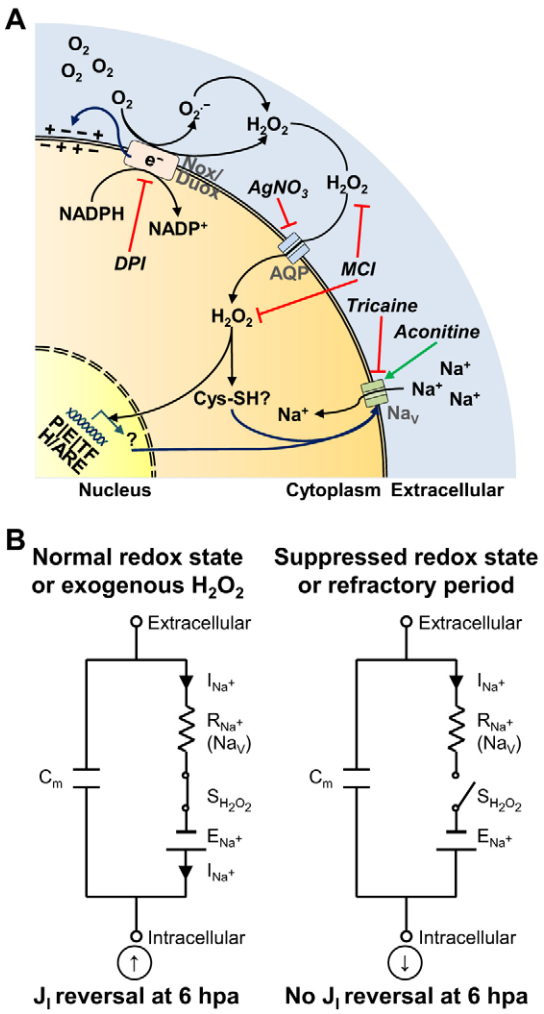

Fig. 6. Biochemical and bioelectrical integration during early regeneration via H_2O_2. (A) Drug targets and H_2O_2 effects on bioelectricity at distinct steps during a putative H_2O_2 'life cycle'. From top to bottom, steps are production of H_2O_2 from NADPH oxidases, availability and diffusion of produced H_2O_2, and H_2O_2-mediated influences on bioelectric activities or parameters (V_m, TEP, EF, J_I and Na_V). A representative cell potentially from wound epithelium (overlaying bud) and/or mesenchymal bud of a tadpole amputated at stage 40-41. It is also possible that one cell produces H_2O_2 and another takes it up to regulate its bioelectric state. For simplicity, we present everything in the same hypothetical cell. e^-, electrons; Nox/Duox, NADPH oxidase families (Nox1, Nox2, Nox4 and Nox5 produce superoxide anion ($O_2^{\cdot-}$), whereas Duox1 and Duox2 produce H_2O_2 directly); AQP, aquaporin; Na_V, voltage-gated Na^+ channel; Cys-SH, cysteine (Cys) residues of proteins containing thiol (-SH) groups suitable for oxidation; P, promoters; E, enhancers; TF, transcription factors; H/ARE, hypoxia and antioxidant responsive elements; black arrows, 'life cycle' of H_2O_2, from upstream O_2 to downstream effect; blue arrows, redox-mediated bioelectric outcome; green arrow, pharmacological activation; red lines, pharmacological inhibition. Drugs are in italic. (B) H_2O_2 is a switcher in the electrical equivalent circuit. Simplified circuit in a membrane patch of, potentially, a wound epithelium (overlaying bud) and/or mesenchymal bud cell of a tadpole amputated during the regenerative (stage 40-41) or refractory (stage 45-46) period. In the absence of H_2O_2 (switcher of Na_V channels), putative Na^+ current (charge carrier) does not cross the membrane through Na_V channels and current reversal does not occur at 6 hpa. Suppressed redox state mimics the refractory period circuit. Exogenous H_2O_2 rescues (from depleted ROS) and induces (from the refractory period) J_I reversal. Na^+, charge carrier; C_m, capacitance of membrane; E_{Na^+}, electromotive force driving Na^+; I_{Na^+}, current of Na^+; R_{Na^+}, resistance to Na^+ flux (synonymous of Na_V channels); $S_{H_2O_2}$, switcher H_2O_2. Arrows inside circles indicate net inward (down arrow) or outward (up arrow) current measured extracellularly.

bioelectricity (Fig. 1, Figs S2-S5) and the temporal requirement for NADPH oxidase-mediated ROS production (Fig. 2A,A′, Fig. S7). These profiles identified the bud at 6 hpa as key to testing the proposed hypothesis, owing to its bioelectric state. Next, we blocked NADPH oxidases and imaged V_m. We found that V_m depolarization resulted from NADPH oxidase activity per se (Fig. 2B,B′). This supported the first part of the two-way regulation hypothesis, arguing that the electrogenic property of NADPH oxidases is the mechanism by which V_m depolarization occurs. As depolarization is not required for regeneration (Adams et al., 2007), we then focused on the extracellular bioelectricity. Drug-depleted ROS levels decreased TEP and prevented or postponed J_I reversal, maintaining a steady outward current at 6 hpa (Fig. 2C,D). This mimicked the altered TEP and J_I measured during the refractory period (Fig. S11). Exogenous H_2O_2 rescued and induced regeneration, TEP and J_I (Figs 2, 3). It also induced ectopic tail formation (Fig. S15). Regeneration efficiency was directly proportional to TEP increase and J_I reversals (Fig. 4, Fig. S14). These results supported the second part of the two-way regulation hypothesis, arguing that H_2O_2 regulates TEP, EF and J_I. Ion translocators are known to mediate bioelectricity (McCaig et al., 2005), thus H_2O_2 is likely to be epistatic to translocators. Indeed, epistasis assays revealed that Na_V channels act downstream of H_2O_2 (Fig. 5). Altogether, the convergent results from disparate methods provide considerable consilience to conclude that redox-modulated regeneration is mediated by early bioelectric activities (Figs 6, 7).

Integrating bioelectric activities in the context of regeneration

Endogenous electric activities arise due to energetically expensive resting electrochemical potentials, primarily V_m and TEP. Can these biological batteries be, in part, dormant sensors and effectors ready to detect and to react to ubiquitous injuries? In fact, the idea that endogenous batteries play a role in wound healing (primarily guiding closure) is not entirely new (Barker et al., 1982; Borgens, 1984; Lykken, 1971). For an integrative view, we propose three phases of extracellular bioelectric contributions in regeneration: passive, active and homeostatic (Fig. 1E, Fig. S5).

Passive (until 6 hpa)

Barrier breaking disrupts the in/out discontinuum so ions leak down their electrochemical gradients, resulting in injury current and lateral EF (primary) with the cathode at the amputation plane. The trunk TEP remains unchanged with amputation, thus the A/P gradient is resolved at this position. Thereby, the 'bioelectric microenvironment' – spatial range of physiologically meaningful bioelectricity – capable of influencing regeneration spans ~335 µm anterior to the amputation plane. Importantly, this microenvironment matches maximum mobilization distances, ~400 µm, of cells for wound closure in urodeles (Lash, 1955).

Active (6-48 hpa, stronger until 24 hpa)

Presumptive barrier restoration re-establishes the discontinuum so ions diffuse with or without energy costs through the wound epithelium. Leaky epithelia are not highly efficient ion-flux barriers due to paracellular movement. Thus, the timing from passive to active activity is difficult to determine precisely. Rather, according to the TEP increase and J_I reversal frequency, a transition should occur from 1 to 6 hpa. Epithelial resistance plus J_I reversal leads to an exponential build-up of TEP, provoking an equivalent drop in EF. The current reversal possibly reversed short-range EF (secondary) locally in the bud (to anode). The plateau

Development (2016) 143, 4582-4594 doi:10.1242/dev.142034

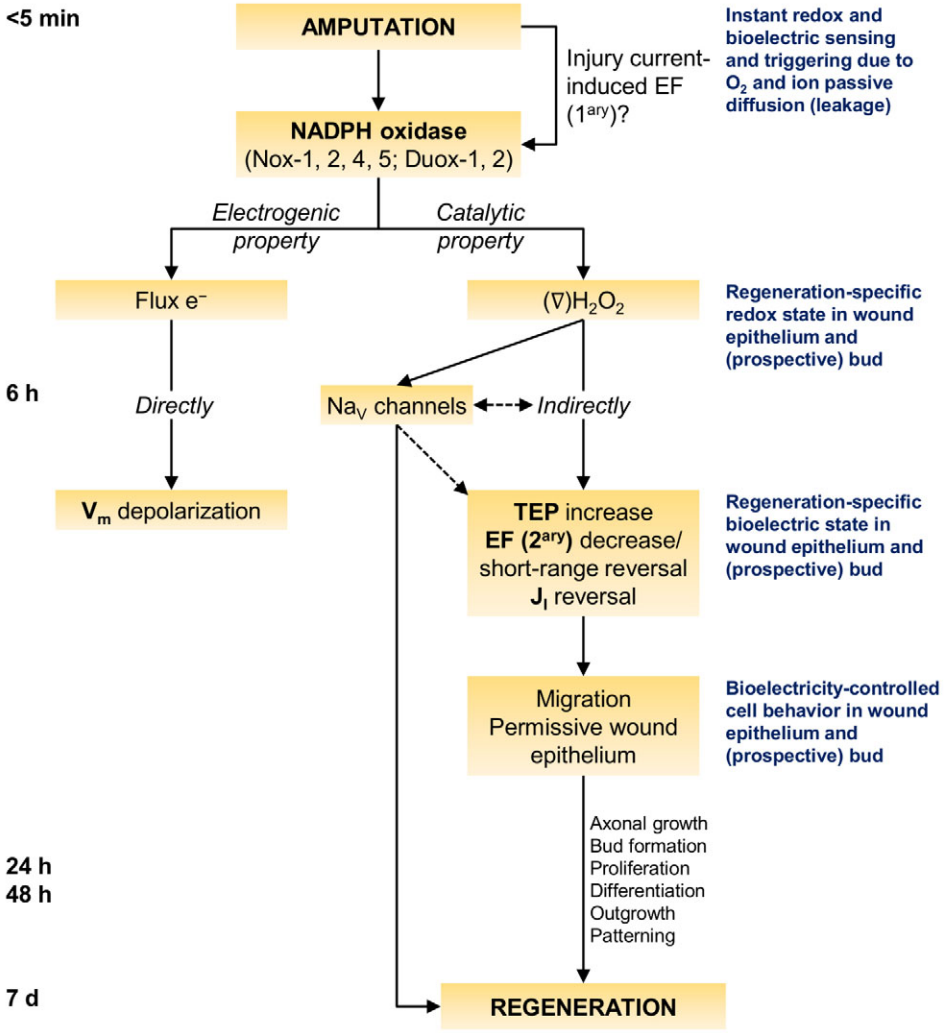

Fig. 7. Stepwise model of redox and bioelectric integration during regeneration. NADPH oxidase-mediated electron flow and H_2O_2 production independently regulate different bioelectric activities. This dual property – electrogenic and catalytic – of NADPH oxidases explicitly represents the proposed two-way regulation hypothesis. The focus is on the early timing of 6 hpa, when the hallmark H_2O_2-switched current reversal occurs in regenerative tadpoles. A redox-bioelectric feedback module may be present, where bioelectric signals (instant primary EF) might activate redox signals (NADPH oxidases and generated H_2O_2), which in turn regulate bioelectricity (V_m, TEP, secondary EF and J_I) to modulate regeneration. Bioelectrically controlled cell migration and subsequent permissive wound epithelium is suggested as a mechanism by which, ultimately, H_2O_2 may control regeneration. e^-, electrons; ∇, gradient.

part in both TEP and J_I suggests that inward current magnitude should go beyond TEP recovery.

Homeostatic (from 48 hpa)

Ion fluxes should now be mainly for housekeeping functions, as TEP and J_I return to uncut baseline, resolving EF. Uncut and complete regeneration tails have an inside-positive TEP and a small inward J_I, in agreement with the salt uptake (osmoregulatory) function of amphibian skin (Koefoed-Johnsen and Ussing, 1958). Remarkably, TEP recovers to the new stage-specific level, not to the level before amputation (Fig. S2C), implying systemic control synchronizing development and regeneration. Bioelectric and regeneration phases dynamically correlate (Figs 1A,E, 4, Fig. S5), suggesting a control of regeneration by bioelectric events.

Is NADPH oxidase-driven V_m depolarization an injury-specific by-product of ROS production?

We showed that the characteristic V_m depolarization in the bud at 6 hpa mechanistically mimics the well-known NADPH oxidase-driven depolarization in immune cells during an oxidative burst (Bankers-Fulbright et al., 2003). This makes it attractive to speculate that V_m depolarization is a by-product of ROS production, which is reinforced by the non-requirement of V_m depolarization for regeneration. V_m should be repolarized by H^+ efflux at 24 hpa to allow regeneration (Adams et al., 2007). We noticed that, irrespective of the drugs used, bud repolarization occurred by 24 hpa (Fig. S8A′), showing that redox state modulates regeneration in a V_m-independent way (Fig. 7). Similarly, robust V_m depolarization around the wound was measured in the caudal fin inter-ray wound model in zebrafish (F.F., unpublished). Importantly, Gauron et al. showed increased ROS levels produced by NADPH oxidases around wounds of the same model (Gauron et al., 2013). Thus, NADPH oxidase-driven V_m depolarization might be a universal injury-specific by-product of ROS production. However, depolarization is not excluded from having functions (Tseng et al., 2010) not addressed in the present study. In the past two decades, non-injury related V_m polarizations are being unveiled as being key in diverse developmental and patterning processes (Levin, 2014). Future work may unveil whether the activities of NADPH oxidases also have a role in these contexts, when ROS production is involved.

Electric current reversal: a potential hallmark of regeneration switched on by H_2O_2

Reid et al. showed a correlation between electric current reversals (from outward to inward) and *X. laevis* tadpole tail regeneration. Ion substitution assays revealed that Na^+ contributed to approximately

Development (2016) 143, 4582-4594 doi:10.1242/dev.142034

two-thirds of the reversed current. However, neither ion nor translocator modulations were able to actually maintain the outward current (Reid et al., 2009). Remarkably, using non-ionic modulation, we either prevented or postponed current reversal in the bud at 6 hpa, mimicking the refractory period. This led to a dramatic inhibition of regeneration. We showed that H_2O_2 diffuses into the cell and stimulates the reversal. Thus, in an electrical equivalent circuit, we propose that H_2O_2 is a switcher that permits Na^+-carried current to diffuse into the stump (Fig. 6B). In the same model, Tseng et al. unveiled part of the molecular basis for Na^+ influx, the channel $Na_V1.2$ (Tseng et al., 2010). We found that H_2O_2 acts upstream of the Na_V channel family. Future work is necessary to reveal the mechanism of this activation, which can be indirect (e.g. redox-sensitive pathways or gene transcription of channels proteins/regulators) or direct (e.g. oxidation of channels cysteine residues, if available) (Fig. 6A). $Na_V1.2$ is present by 18 hpa in the bud, accumulating cations there (Tseng et al., 2010). The mismatch with our measured reversal at 6 hpa might imply other Na_V channel(s) in action, possibly in the wound epithelium. This would complete the path of Na^+ from outside to bud, as barrier restoration prevents most ion leakage and reduces paracellular flux. In principle, however, some Na^+ transporter(s) should be present in the wound epithelium to move the ions against the electrochemical gradient. The sharp TEP increase until 6 hpa supports this and might suggest the ubiquitous Na^+/K^+-ATPase as a candidate (Dubé et al., 2010). Thus, it is possible that H_2O_2 (or other ROS) modulates additional ion translocators (Ma, 2011; Matalon et al., 2003). Exogenous H_2O_2 rescued and induced regeneration and induced ectopic tails, suggesting that H_2O_2 provides indispensable morphogenetic information. H_2O_2 robustly rescued and induced TEP increase and J_I reversal at 6 hpa. Therefore, we propose that H_2O_2-switched current reversal is a hallmark of regeneration. As a limiting and stimulating factor of regeneration, this hallmark can be used as a diagnostic characteristic of regeneration and as a marker and prognosis of its efficiency (Fig. 4). Furthermore, it can be used to promote regeneration in regenerative-deficient animals.

J_I reversal prior to blastema formation was also seen in newt limbs (unquantified frequency, apparently occasional due to net outward current) (Borgens et al., 1977b) and tails (Nawata, 2001), and in *X. laevis* tadpole limb regeneration (G.L., unpublished). Reversal in newt tails was assumed to be a return to baseline (Nawata, 2001), despite the higher magnitude than before amputation. Surface potential measurements revealed stump potential reversal (from positive to negative) prior to blastema formation in urodels, but not in non-permissive anuran limb regeneration (Becker, 1961; Rose and Rose, 1974), showing a correlation with regeneration. However, another study found potential reversal in both taxa (Lassalle, 1979). We measured instead transepithelial potentials that, apart from sporadic reversals, had no overall mean reversal. Short-range $EF_{Shoulder \rightarrow Bud}$ presented more reversal frequency (21%) than did long-range $EF_{Trunk \rightarrow Bud}$ (9%) at 6 hpa (increasing thereafter; Fig. S3C), indicating the predominance of local reversal (in the bud). Indeed, in newt limbs, the surface potential reversal occurred only a short distance from the amputation plane (Rose and Rose, 1974). The small and soft bud hindered the spatial resolution required to fully characterize local reversals. Unambiguous current reversal supports the short-range potential and EF reversals in the bud. Altogether, our results showed a close correlation between reversals, bud formation and regeneration (Figs 4, 6, 7).

How can the H_2O_2-switched current reversal mechanistically impact regeneration? Cell migration precedes proliferation (Adams et al., 2007) and is essential for wound closure in the first phase of regeneration (Beck et al., 2009). Thus, the early and vectorial J_I reversal suggests migration as a prime candidate. However, other cell behaviors are not excluded. Cumulative evidence shows that endogenous or exogenous EF act as guiding cues for migration during wound healing (McCaig et al., 2005; Zhao et al., 1996, 2006). Importantly, most cells, including keratinocytes and neurons, migrate or grow towards the cathode (Song, 2004; Sun et al., 2013). ROS-depleted and refractory period tails at 6 hpa had a sustained outward J_I that led to lower bud TEP and higher short-range EF, establishing a long-term cathode at amputation plane (Figs 2C, 3B, Figs S11, S16A). Therefore, we postulate that a non-reversed J_I by 6 hpa might lead to cell overmigration. In short, cells are deluded into behaving as if the wound was still open (Fig. S16B). Wound epithelium from the refractory period is thicker than regenerative *X. laevis* tadpole tails (Beck et al., 2003; Reid et al., 2009; Tseng et al., 2010). Mature skin flapped or grafted to amputated newt limbs or children's fingertips blocks regeneration (Illingworth, 1974; Mescher, 1976). Interestingly, these skin-like structures have altered currents (Altizer et al., 2002; Reid et al., 2009) (Fig. S11) and might disrupt epithelial-mesenchymal crosstalk (Lee et al., 2009), both of which are important for regeneration. Thereby, cell overmigration might produce a non-permissive refractory-like wound epithelium. This might explain why J_I reversal by 24 hpa in MCI- and $AgNO_3$-treated tails (Fig. S8C) was not sufficient for regeneration (Fig. 2A,A′). Although we cannot exclude direct ROS-induced chemotaxis (Hurd et al., 2012; Pan et al., 2011), ROS-modulated electrotaxis might be the major cue (Zhao, 2009). This rationale could apply to axonal sprouting and to axonal growth (electrotropism). Neuronal presence is a long-recognized limiting and stimulating factor in regeneration (Kumar and Brockes, 2012; Sidman and Singer, 1951). Importantly, applied currents enhance nerve growth and regeneration in adult frogs (Borgens et al., 1979). Observed J_I reversal per se or the establishment of a steady inward current might be independent cues. Reversal can be a transitory electric pole discretely sensed by cells. Therefore, J_I reversal may fine-tune (mitigate) migration of cells and axonal growth, setting the conditions for or triggering bud initiation around 6 hpa and subsequent proliferation and *de novo* tail formation. Indeed, a permissive epithelium neuronally supplied (Thornton, 1954) is the basis of the accessory limb formation in axolotls (Endo et al., 2004). H_2O_2-induced ectopic tails might thus result from bioelectric effects on neuronal tissue.

Towards a comprehensive model of redox and bioelectric integration during regeneration

We aimed to conceptualize a comprehensive model that integrates redox and bioelectric states during regeneration (Fig. 7). We showed that NADPH oxidase-mediated ROS production is pleiotropic (early on it affects morphogenesis; later on it affects growth) and is required immediately upon amputation. Thus, an elusive ultra-fast signal needs to trigger the activity of NADPH oxidases. Probably the fastest injury-induced signals are bioelectric in nature. Exogenous EF activate NADPH oxidases in cells *in vitro* (Chatterjee et al., 2012; Li et al., 2013). Thus, we propose that endogenous EF activate NADPH oxidases (Fig. 7). Another candidate is Ca^{2+} signaling. Wounding induces fast Ca^{2+} influx and Ca^{2+} flashes in *X. laevis* oocytes and *Drosophila* embryo, respectively (Luxardi et al., 2014; Razzell et al., 2013). Importantly, those flashes activate a NADPH oxidase (Duox). Excitingly, this points to a feedback module, where bioelectric signals (primary EF and/or Ca^{2+}) might activate redox signals (NADPH oxidases and generated H_2O_2) that in turn regulate bioelectricity (V_m, TEP,

Development (2016) 143, 4582-4594 doi:10.1242/dev.142034

secondary EF and J_I) to modulate regeneration (Fig. 7). This might be a starting point from which to test whether bioelectricity-modulated redox activities also occur during regeneration. By 6 hpa, the electrogenic property of NADPH oxidases depolarizes V_m and the catalytic property stimulates TEP recovery and switches on J_I reversal (Figs 6B, 7). H_2O_2-modulated regeneration is then V_m independent. However, both paths might interact. For example, preventing V_m repolarization downregulates $Na_V1.2$ expression (Tseng et al., 2010). H_2O_2 diffusion into cells revealed for the first time, to our knowledge, that aquaporins are potential new targets to modulate epimorphic regeneration (Fig. 6A). H_2O_2-switched current reversal, potentially via Na_V channels, may fine-tune cell migration and axonal growth that is essential for regeneration (Figs 6, 7).

Although the evidence supporting H_2O_2 is compelling, the role of other ROS in controlling bioelectric and regenerative outcomes should not be excluded (Li et al., 2013). Moreover, the possible importance of a H_2O_2 extracellular gradient is not excluded by this study. Indeed, it might be translated into a gradient of bioelectric activity that can be a blueprint for positional information and axes patterning (Jaffe, 1981; Tseng and Levin, 2013). Engineered solutions for controlled release of H_2O_2 (Garland et al., 2014) may prove useful for future work, especially in non-aquatic models.

In conclusion, this study unveils the interplay between biochemical and biophysical signals during regeneration, suggesting a novel mechanism that mediates regeneration: early H_2O_2-switched J_I reversal, potentially via Na_V channels. It also highlights the opportunities for interdisciplinary integration of apparently disparate states (Serena et al., 2009; Tandon et al., 2014) that may reserve promising advances for translational medicine.

MATERIALS AND METHODS

Animals and surgery

Animal procedures and pharmacological treatments were approved by local Institutional Animal Care and Use Committee (protocols 16822 and 18601). *Xenopus laevis* (Daudin, 1802) tadpoles acquired from Xenopus Express (www.xenopus.com) were staged (Nieuwkoop and Faber, 1967), sorted and transferred to fresh Marc's modified Ringer (MMR) 0.1× culture medium, composed of (in mM): NaCl 10, $CaCl_2{\cdot}2H_2O$ 0.2, KCl 0.2, $MgCl_2{\cdot}6H_2O$ 0.1 and HEPES 0.5 (pH 7.1-7.2) (Sigma-Aldrich). Surgery was executed as previously described (Adams et al., 2007; Reid et al., 2009). For further details, see Supplementary Materials and Methods.

Tail regeneration assay

Tail regeneration assays were performed as previously described (Adams et al., 2007; Tseng et al., 2010). For further details, see Supplementary Materials and Methods.

Ectopic tail induction

Ectopic tails were induced by a dorsal incision severing down to the spinal cord (inclusive; Fig. S15A) (Sugiura et al., 2009). For further details, see Supplementary Materials and Methods.

Pharmacological modulations

Drugs and respective vehicle reconstituted in MMR 0.1× were applied via immersion (bath) at the doses and exposures specified. Most drugs were stocked in DMSO (Sigma-Aldrich, cat. no. D2650) at −20°C: DPI (Sigma-Aldrich, cat. no. D2926) 1 and 10 mM; MCI (Cayman chemical, cat. no. 13320) 200 mM; $AgNO_3$ (Sigma-Aldrich, cat. no. 209139) 24 mM; apocynin (Sigma-Aldrich, cat. no. W508454) 200 mM; VAS (EMD Millipore, cat. no. 492000) 1.4 mM; and aconitine (Alamone Labs, cat. no. A-150) 1 mM. Vehicle (DMSO) had non-significant effects on readouts (Fig. S1). H_2O_2 (EMD Millipore, cat. no. HX0635) was kept as a 1 M stock in deionized water at 4°C. Occasionally, stocks of 25 and 50 mM were kept for short periods at −20°C. Tricaine was kept as a 1 mM stock in MMR 0.1× (pH readjusted to 7.2) at −20°C. Working solutions were freshly prepared. For further details, see Supplementary Materials and Methods.

ROS and V_m fluorescence imaging

Intracellular relative ROS and V_m were measured non-invasively by fluorescence imaging of vital dyes as previously described (Adams et al., 2007; Owusu-Ansah et al., 2008). For further details, see Supplementary Materials and Methods.

Glass microelectrode measurement

Transepithelial potential was measured invasively by glass microelectrode impalement through the epithelial layers as previously described (Luxardi et al., 2014; McCaig and Robinson, 1982). For further details, see Supplementary Materials and Methods.

Vibrating probe measurement

Extracellular net electric current density was measured non-invasively with a locked-in one dimensional vibrating probe, prepared and used as previously described (Reid et al., 2007, 2009). For further details, see Supplementary Materials and Methods.

Statistical analysis

Regeneration efficiencies were compared using the Fisher's exact test. Frequencies (in J_I reversals and ectopic tails) were compared using the Mann-Whitney *U*-test. Correlations were tested with the Pearson's correlation coefficient *r*. Linear regressions (coefficient of determination r^2) were applied to fit data to a statistical model. All remaining comparisons were analyzed using the unpaired Student's *t*-test.

Data are presented as mean±s.e.m. Sample size (*n*, biological replicates) used in each experiment are stated in figures and text. At least two independent batches of tadpoles were used per readout. Differences were significant if $P<0.05$ and the levels of significance are: NS, non-significant; $*P<0.05$; $**P<0.01$ and $***P<0.001$. Means and standard errors were calculated and plotted using Excel, and statistics were performed using GraphPad Prism 5 (GraphPad Software). For further details, see Supplementary Materials and Methods.

Acknowledgements

We apologize for not being able to cite all the relevant studies due to space or context constraints. We are grateful to Dr Andreia Gomes (Departamento de Biologia, CBMA, Universidade do Minho, Portugal) and to Dr VijayKrishna Raghunathan [Department of Surgical and Radiological Sciences, University of California (UC) Davis; The Ocular Surface Institute, College of Optometry, University of Houston, TX, USA] for helpful discussion. We thank Dr Paul Fitzgerald (Department of Cell Biology and Human Anatomy, UC Davis) and Dr Andrew Ishida [Department of Neurobiology, Physiology, and Behavior (NPB), UC Davis] for providing access to confocal microscopes. We are grateful to Dr Tyler Stradleighand (Department of NPB, UC Davis) and to Dr Qizhi Gong (Department of Cell Biology and Human Anatomy, UC Davis) for training and suggestions in confocal microscopy. We thank Dr Yao-Hui Sun for providing zebrafish and all other lab members (past and present) for helpful discussion.

Competing interests

The authors declare no competing or financial interests.

Author contributions

F.F. and M.Z. conceived the study. F.F., G.L. and M.Z. designed the experiments. F.F. performed the experiments and analyzed the results. G.L. and B.R. provided technical training and guidance, and helped to interpret some results. F.F., G.L. and M.Z. outlined the manuscript. F.F. wrote the manuscript. All authors read, commented and agreed with the final version of the manuscript.

Funding

This work was supported by the UC Davis Principal Investigator Bridge Program and the National Institutes of Health (EB015737), and, in part, by an unrestricted grant from Research to Prevent Blindness from UC Davis Ophthalmology. F.F. was supported by Fundação para a Ciência e a Tecnologia (SFRH/BD/87256/2012). Deposited in PMC for release after 12 months.

Development (2016) 143, 4582-4594 doi:10.1242/dev.142034

Supplementary information

Supplementary information available online at
http://dev.biologists.org/lookup/doi/10.1242/dev.142034.supplemental

References

Adams, D. S., Masi, A. and Levin, M. (2007). H+ pump-dependent changes in membrane voltage are an early mechanism necessary and sufficient to induce Xenopus tail regeneration. *Development* **134**, 1323-1335.

Altizer, A. M., Stewart, S. G., Albertson, B. K. and Borgens, R. B. (2002). Skin flaps inhibit both the current of injury at the amputation surface and regeneration of that limb in newts. *J. Exp. Zool.* **293**, 467-477.

Alvarado, A. S. and Tsonis, P. A. (2006). Bridging the regeneration gap: genetic insights from diverse animal models. *Nat. Rev. Genet.* **7**, 873-884.

Ameri, A. (1998). The effects of Aconitum alkaloids on the central nervous system. *Prog. Neurobiol.* **56**, 211-235.

Bankers-Fulbright, J. L., Gleich, G. J., Kephart, G. M., Kita, H. and O'Grady, S. M. (2003). Regulation of eosinophil membrane depolarization during NADPH oxidase activation. *J. Cell Sci.* **116**, 3221-3226.

Barker, A. T., Jaffe, L. F. and Vanable, J. W. (1982). The glabrous epidermis of cavies contains a powerful battery. *Am. J. Physiol.* **242**, R358-R366.

Beane, W. S., Morokuma, J., Adams, D. S. and Levin, M. (2011). A chemical genetics approach reveals H,K-ATPase-mediated membrane voltage is required for planarian head regeneration. *Chem. Biol.* **18**, 77-89.

Beck, C. W., Christen, B. and Slack, J. M. W. (2003). Molecular pathways needed for regeneration of spinal cord and muscle in a vertebrate. *Dev. Cell* **5**, 429-439.

Beck, C. W., Izpisúa Belmonte, J. C. and Christen, B. (2009). Beyond early development: Xenopus as an emerging model for the study of regenerative mechanisms. *Dev. Dyn.* **238**, 1226-1248.

Becker, R. O. (1961). The bioelectric factors regeneration in amphibian-limb regeneration. *J. Bone Jt. Surg.* **43**, 643-656.

Becker, R. O. (1972). Stimulation of partial limb regeneration in rats. *Nature* **235**, 109-111.

Bienert, G. P. and Chaumont, F. (2014). Aquaporin-facilitated transmembrane diffusion of hydrogen peroxide. *Biochim. Biophys. Acta* **1840**, 1596-1604.

Borgens, R. B. (1984). Are limb development and limb regeneration both initiated by an integumentary wounding? A hypothesis. *Differentiation* **28**, 87-93.

Borgens, R. B., Vanable, J. W. and Jaffe, L. F. (1977a). Bioelectricity and regeneration. I. Initiation of frog limb regeneration by minute currents. *J. Exp. Zool.* **200**, 403-416.

Borgens, R. B., Vanable, J. W. and Jaffe, L. F. (1977b). Bioelectricity and regeneration: large currents leave the stumps of regenerating newt limbs. *Proc. Natl. Acad. Sci. USA* **74**, 4528-4532.

Borgens, R. B., Vanable, J. W. and Jaffe, L. F. (1979). Small artificial currents enhance Xenopus limb regeneration. *J. Exp. Zool.* **207**, 217-226.

Chatterjee, S., Browning, E. A., Hong, N., DeBolt, K., Sorokina, E. M., Liu, W., Birnbaum, M. J. and Fisher, A. B. (2012). Membrane depolarization is the trigger for PI3K/Akt activation and leads to the generation of ROS. *AJP Hear. Circ. Physiol.* **302**, H105-H114.

Demaurex, N. and Petheö, G. L. (2005). Electron and proton transport by NADPH oxidases. *Philos. Trans. R. Soc. Lond. B. Biol. Sci.* **360**, 2315-2325.

Deuchar, E. M. (1975). Regeneration of the tail bud in Xenopus embryos. *J. Exp. Zool.* **192**, 381-389.

Dubé, J., Rochette-Drouin, O., Lévesque, P., Gauvin, R., Roberge, C. J., Auger, F. A., Goulet, D., Bourdages, M., Plante, M., Germain, L. et al. (2010). Restoration of the transepithelial potential within tissue-engineered human skin in vitro and during the wound healing process in vivo. *Tissue Eng. Part A* **16**, 3055-3063.

Endo, T., Bryant, S. V. and Gardiner, D. M. (2004). A stepwise model system for limb regeneration. *Dev. Biol.* **270**, 135-145.

Frazier, D. T. and Narahashi, T. (1975). Tricaine (MS-222): effects on ionic conductances of squid axon membranes. *Eur. J. Pharmacol.* **33**, 313-317.

Garland, S. P., Wang, R. Y., Raghunathan, V. K., Lam, K. S., Murphy, C. J., Russell, P., Sun, G. and Pan, T. (2014). Photopatternable and photoactive hydrogel for on-demand generation of hydrogen peroxide in cell culture. *Biomaterials* **35**, 1762-1770.

Gauron, C., Rampon, C., Bouzaffour, M., Ipendey, E., Teillon, J., Volovitch, M. and Vriz, S. (2013). Sustained production of ROS triggers compensatory proliferation and is required for regeneration to proceed. *Sci. Rep.* **3**, 2084.

Golding, A., Guay, J. A., Herrera-Rincon, C., Levin, M. and Kaplan, D. L. (2016). A tunable silk hydrogel device for studying limb regeneration in adult Xenopus Laevis. *PLoS ONE* **11**, e0155618.

Han, P., Zhou, X.-H., Chang, N., Xiao, C.-L., Yan, S., Ren, H., Yang, X.-Z., Zhang, M.-L., Wu, Q., Tang, B. et al. (2014). Hydrogen peroxide primes heart regeneration with a derepression mechanism. *Cell Res.* **24**, 1091-1107.

Hechavarria, D., Dewilde, A., Braunhut, S., Levin, M. and Kaplan, D. L. (2010). BioDome regenerative sleeve for biochemical and biophysical stimulation of tissue regeneration. *Med. Eng. Phys.* **32**, 1065-1073.

Hurd, T. R., DeGennaro, M. and Lehmann, R. (2012). Redox regulation of cell migration and adhesion. *Trends Cell Biol.* **22**, 107-115.

Illingworth, C. M. (1974). Trapped fingers and amputated finger tips in children. *J. Pediatr. Surg.* **9**, 853-858.

Jaffe, L. F. (1981). The role of ionic currents in establishing developmental pattern. *Philos. Trans. R. Soc. Lond. B. Biol. Sci.* **295**, 553-566.

Jenkins, L. S., Duerstock, B. S. and Borgens, R. B. (1996). Reduction of the current of injury leaving the amputation inhibits limb regeneration in the red spotted newt. *Dev. Biol.* **178**, 251-262.

Koefoed-Johnsen, V. and Ussing, H. H. (1958). The nature of the frog skin potential. *Acta Physiol. Scand.* **42**, 298-308.

Kumar, A. and Brockes, J. P. (2012). Nerve dependence in tissue, organ, and appendage regeneration. *Trends Neurosci.* **35**, 691-699.

Lambeth, J. D. and Neish, A. S. (2014). Nox enzymes and new thinking on reactive oxygen: a double-edged sword revisited. *Annu. Rev. Pathol.* **9**, 119-145.

Lash, J. W. (1955). Studies on wound closure in urodeles. *J. Exp. Zool.* **128**, 13-28.

Lassalle, B. (1979). Surface potentials and the control of amphibian limb regeneration. *J. Embryol. Exp. Morphol.* **53**, 213-223.

Lee, Y., Hami, D., De Val, S., Kagermeier-Schenk, B., Wills, A. A., Black, B. L., Weidinger, G. and Poss, K. D. (2009). Maintenance of blastemal proliferation by functionally diverse epidermis in regenerating zebrafish fins. *Dev. Biol.* **331**, 270-280.

Leppik, L. P., Froemel, D., Slavici, A., Ovadia, Z. N., Hudak, L., Henrich, D., Marzi, I. and Barker, J. H. (2015). Effects of electrical stimulation on rat limb regeneration, a new look at an old model. *Sci. Rep.* **5**, 18353.

Levin, M. (2007). Large-scale biophysics: ion flows and regeneration. *Trends Cell Biol.* **17**, 261-270.

Levin, M. (2014). Molecular bioelectricity: how endogenous voltage potentials control cell behavior and instruct pattern regulation in vivo. *Mol. Biol. Cell* **25**, 3835-3850.

Li, F., Chen, T., Hu, S., Lin, J., Hu, R. and Feng, H. (2013). Superoxide mediates direct current electric field-induced directional migration of glioma cells through the activation of AKT and ERK. *PLoS ONE* **8**, e61195.

Loo, A. E. K., Wong, Y. T., Ho, R., Wasser, M., Du, T., Ng, W. T. and Halliwell, B. (2012). Effects of hydrogen peroxide on wound healing in mice in relation to oxidative damage. *PLoS ONE* **7**, e49215.

Love, N. R., Chen, Y., Ishibashi, S., Kritsiligkou, P., Lea, R., Koh, Y., Gallop, J. L., Dorey, K. and Amaya, E. (2013). Amputation-induced reactive oxygen species are required for successful Xenopus tadpole tail regeneration. *Nat. Cell Biol.* **15**, 222-228.

Luxardi, G., Reid, B., Maillard, P. and Zhao, M. (2014). Single cell wound generates electric current circuit and cell membrane potential variations that requires calcium influx. *Integr. Biol.* **6**, 662-672.

Lykken, D. T. (1971). Square-wave analysis of skin impedance. *Psychophysiology* **7**, 262-275.

Ma, H.-P. (2011). Hydrogen peroxide stimulates the epithelial sodium channel through a phosphatidylinositide 3-kinase-dependent pathway. *J. Biol. Chem.* **286**, 32444-32453.

Matalon, S., Hardiman, K. M., Jain, L., Eaton, D. C., Kotlikoff, M., Eu, J. P., Sun, J., Meissner, G., Stamler, J. S., Hardiman, K. M. et al. (2003). Regulation of ion channel structure and function by reactive oxygen-nitrogen species. *Am. J. Physiol. Lung Cell. Mol. Physiol.* **285**, L1184-L1189.

McCaig, C. D. and Robinson, K. R. (1982). The ontogeny of the transepidermal potential difference in frog embryos. *Dev. Biol.* **90**, 335-339.

McCaig, C. D., Rajnicek, A. M., Song, B. and Zhao, M. (2005). Controlling cell behavior electrically: current views and future potential. *Physiol. Rev.* **85**, 943-978.

McGinnis, M. E. and Vanable, J. W. (1986). Electrical fields in Notophthalmus viridescens limb stumps. *Dev. Biol.* **116**, 184-193.

Mescher, A. L. (1976). Effects on adult newt limb regeneration of partial and complete skin flaps over the amputation surface. *J. Exp. Zool.* **195**, 117-127.

Miller, E. W., Dickinson, B. C. and Chang, C. J. (2010). Aquaporin-3 mediates hydrogen peroxide uptake to regulate downstream intracellular signaling. *Proc. Natl. Acad. Sci. USA* **107**, 15681-15686.

Monteiro, J., Aires, R., Becker, J. D., Jacinto, A., Certal, A. C. and Rodríguez-León, J. (2014). V-ATPase proton pumping activity is required for adult zebrafish appendage regeneration. *PLoS ONE* **9**, e92594.

Moreira, S., Stramer, B., Evans, I., Wood, W. and Martin, P. (2010). Prioritization of competing damage and developmental signals by migrating macrophages in the Drosophila embryo. *Curr. Biol.* **20**, 464-470.

Nawata, T. (2001). Wound currents following amputation of tail tip in the Japanese Newt, Cynops pyrrhogaster. *Zoolog. Sci.* **18**, 11-15.

Niemietz, C. M. and Tyerman, S. D. (2002). New potent inhibitors of aquaporins: silver and gold compounds inhibit aquaporins of plant and human origin. *FEBS Lett.* **531**, 443-447.

Niethammer, P., Grabher, C., Look, A. T. and Mitchison, T. J. (2009). A tissue-scale gradient of hydrogen peroxide mediates rapid wound detection in zebrafish. *Nature* **459**, 996-999.

Nieuwkoop, P. D. and Faber, J. (1967). *Normal Table of Xenopus laevis (Daudin)*. Amsterdam: North-Holland.

O'Donnell, V. B., Tew, D. G., Jones, O. T. G. and England, P. J. (1993). Studies on the inhibitory mechanism of iodonium compounds with special reference to neutrophil NADPH oxidase. *Biochem. J.* **290**, 41-49.

Otomo, E. (2003). Effect of a novel free radical scavenger, edaravone (MCI-186), on acute brain infarction. Randomized, placebo-controlled, double-blind study at multicenters. *Cerebrovasc. Dis.* **15**, 222-229.
Owusu-Ansah, E., Yavari, A., Mandal, S. and Banerjee, U. (2008). Distinct mitochondrial retrograde signals control the G1-S cell cycle checkpoint. *Nat. Genet.* **40**, 356-361.
Özkucur, N., Epperlein, H.-H. and Funk, R. H. W. (2010). Ion imaging during axolotl tail regeneration in vivo. *Dev. Dyn.* **239**, 2048-2057.
Pan, Q., Qiu, W.-Y., Huo, Y.-N., Yao, Y.-F. and Lou, M. F. (2011). Low levels of hydrogen peroxide stimulate corneal epithelial cell adhesion, migration, and wound healing. *Invest. Ophthalmol. Vis. Sci.* **52**, 1723-1734.
Pirotte, N., Stevens, A.-S., Fraguas, S., Plusquin, M., Van Roten, A., Van Belleghem, F., Paesen, R., Ameloot, M., Cebrià, F., Artois, T. et al. (2015). Reactive oxygen species in planarian regeneration: an upstream necessity for correct patterning and brain formation. *Oxid. Med. Cell. Longev.* **2015**, 1-19.
Razzell, W., Evans, I. R., Martin, P. and Wood, W. (2013). Calcium flashes orchestrate the wound inflammatory response through duox activation and hydrogen peroxide release. *Curr. Biol.* **23**, 424-429.
Reid, B., Nuccitelli, R. and Zhao, M. (2007). Non-invasive measurement of bioelectric currents with a vibrating probe. *Nat. Protoc.* **2**, 661-669.
Reid, B., Song, B. and Zhao, M. (2009). Electric currents in Xenopus tadpole tail regeneration. *Dev. Biol.* **335**, 198-207.
Rose, M. S. and Rose, F. C. (1974). Electrical studies on normally regenerating, on X-rayed, and on denervated limb stumps of Triturus. *Growth* **38**, 363-380.
Sen, C. K. and Roy, S. (2008). Redox signals in wound healing. *Biochim. Biophys. Acta* **1780**, 1348-1361.
Serena, E., Figallo, E., Tandon, N., Cannizzaro, C., Gerecht, S., Elvassore, N. and Vunjak-Novakovic, G. (2009). Electrical stimulation of human embryonic stem cells: cardiac differentiation and the generation of reactive oxygen species. *Exp. Cell Res.* **315**, 3611-3619.
Shapiro, S., Borgens, R., Pascuzzi, R., Roos, K., Groff, M., Purvines, S., Rodgers, R. B., Hagy, S. and Nelson, P. (2005). Oscillating field stimulation for complete spinal cord injury in humans: a phase 1 trial. *J. Neurosurg. Spine* **2**, 3-10.
Sidman, R. L. and Singer, M. (1951). Stimulation of forelimb regeneration in the newt, Triturus viridescens, by a sensory nerve supply isolated from the central nervous system. *Am. J. Physiol.* **165**, 257-260.
Simons, J. M., 't Hart, B. A., Ip Vai Ching, T. R. A. M., Van Dijk, H. and Labadie, R. P. (1990). Metabolic activation of natural phenols into selective oxidative burst agonists by activated human neutrophils. *Free Radic. Biol. Med.* **8**, 251-258.
Smith, S. D. (1967). Induction of partial limb regeneration in Rana pipiens by galvanic stimulation. *Anat. Rec.* **158**, 89-97.
Song, B., Zhao, M., Forrester, J. and McCaig, C. (2004). Nerve regeneration and wound healing are stimulated and directed by an endogenous electrical field in vivo. *J. Cell Sci.* **117**, 4681-4690.
Stoick-Cooper, C. L., Moon, R. T. and Weidinger, G. (2007). Advances in signaling in vertebrate regeneration as a prelude to regenerative medicine. *Genes Dev.* **21**, 1292-1315.
Sugiura, T., Tazaki, A., Ueno, N., Watanabe, K. and Mochii, M. (2009). Xenopus Wnt-5a induces an ectopic larval tail at injured site, suggesting a crucial role for noncanonical Wnt signal in tail regeneration. *Mech. Dev.* **126**, 56-67.
Sun, Y., Do, H., Gao, J., Zhao, R., Zhao, M. and Mogilner, A. (2013). Keratocyte fragments and cells utilize competing pathways to move in opposite directions in an electric field. *Curr. Biol.* **23**, 569-574.
Tandon, N., Cimetta, E., Villasante, A., Kupferstein, N., Southall, M. D., Fassih, A., Xie, J., Sun, Y. and Vunjak-Novakovic, G. (2014). Galvanic microparticles increase migration of human dermal fibroblasts in a wound-healing model via reactive oxygen species pathway. *Exp. Cell Res.* **320**, 79-91.
ten Freyhaus, H., Huntgeburth, M., Wingler, K., Schnitker, J., Bäumer, A. T., Vantler, M., Bekhite, M. M., Wartenberg, M., Sauer, H. and Rosenkranz, S. (2006). Novel Nox inhibitor VAS2870 attenuates PDGF-dependent smooth muscle cell chemotaxis, but not proliferation. *Cardiovasc. Res.* **71**, 331-341.
Thornton, C. S. (1954). The relation of epidermal innervation to limb regeneration in Amblystoma larvae. *J. Exp. Zool.* **127**, 577-601.
Tseng, A.-S. and Levin, M. (2013). Cracking the bioelectric code: Probing endogenous ionic controls of pattern formation. *Commun. Integr. Biol.* **6**, 1-8.
Tseng, A.-S., Beane, W. S., Lemire, J. M., Masi, A. and Levin, M. (2010). Induction of vertebrate regeneration by a transient sodium current. *J. Neurosci.* **30**, 13192-13200.
Veal, E. A., Day, A. M. and Morgan, B. A. (2007). Hydrogen peroxide sensing and signaling. *Mol. Cell* **26**, 1-14.
Verkman, A. S., Anderson, M. O. and Papadopoulos, M. C. (2014). Aquaporins: important but elusive drug targets. *Nat. Rev. Drug Discov.* **13**, 259-277.
Wittmann, C., Chockley, P., Singh, S. K., Pase, L., Lieschke, G. J. and Grabher, C. (2012). Hydrogen peroxide in inflammation: messenger, guide, and assassin. *Adv. Hematol.* **2012**, 541471.
Yoo, S. K., Starnes, T. W., Deng, Q. and Huttenlocher, A. (2011). Lyn is a redox sensor that mediates leukocyte wound attraction in vivo. *Nature* **480**, 109-112.
Yoo, S. K., Freisinger, C. M., LeBert, D. C. and Huttenlocher, A. (2012). Early redox, Src family kinase, and calcium signaling integrate wound responses and tissue regeneration in zebrafish. *J. Cell Biol.* **199**, 225-234.
Zhang, Q., Wang, Y., Man, L., Zhu, Z., Bai, X., Wei, S., Liu, Y., Liu, M., Wang, X., Gu, X. et al. (2016). Reactive oxygen species generated from skeletal muscles are required for gecko tail regeneration. *Sci. Rep.* **6**, 1-11.
Zhao, M. (2009). Electrical fields in wound healing—an overriding signal that directs cell migration. *Semin. Cell Dev. Biol.* **20**, 674-682.
Zhao, M., Agius-Fernandez, A., Forrester, J. V. and McCaig, C. D. (1996). Orientation and directed migration of cultured corneal epithelial cells in small electric fields are serum dependent. *J. Cell Sci.* **109**, 1405-1414.
Zhao, M., Song, B., Pu, J., Wada, T., Reid, B., Tai, G., Wang, F., Guo, A., Walczysko, P., Gu, Y. et al. (2006). Electrical signals control wound healing through phosphatidylinositol-3-OH kinase-gamma and PTEN. *Nature* **442**, 457-460.

Supplementary Information

Supplementary Figures

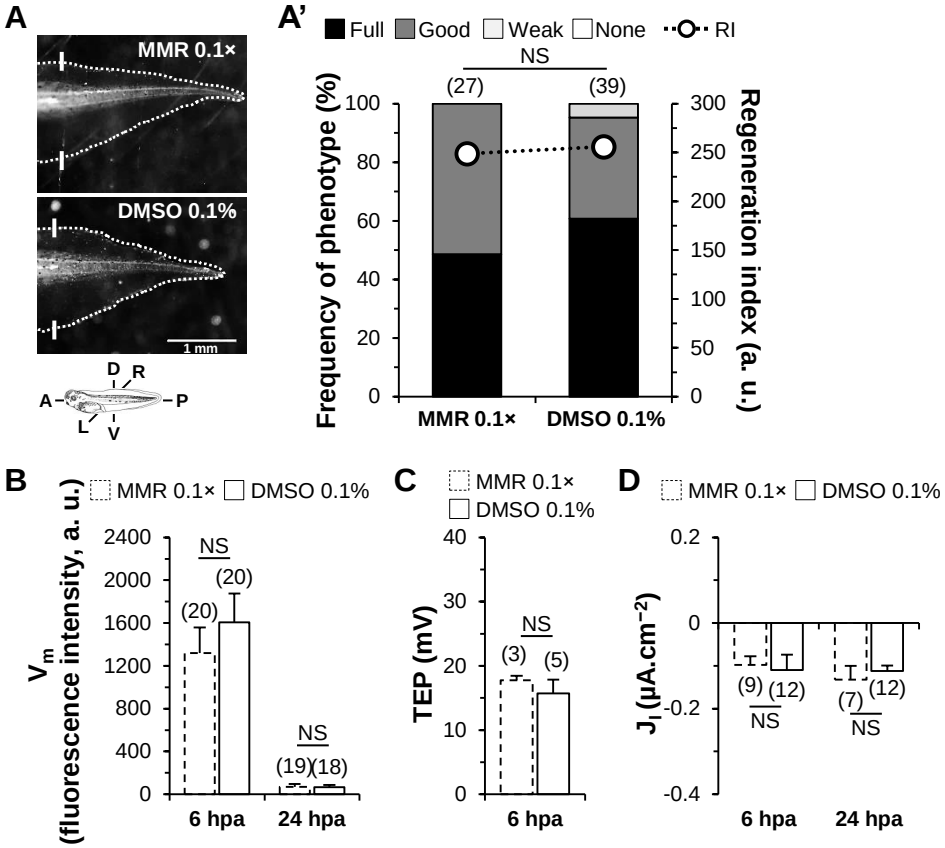

Fig. S1. Vehicle-control does not affect regeneration or V_m, TEP and J_I. (**A,A'**) Vehicle-control (DMSO 0.1%) does not affect regeneration. (**A**) Representative 7 dpa tails of control (MMR 0.1×) and of vehicle-control (DMSO 0.1%). Photomicrographs of regenerating or regenerated tails are displayed in the same orientation as the whole organism anteroposterior (A/P), dorsoventral (D/V) and left-right (L/R) axes (bottom scheme; applies to subsequent figures). White solid lines: amputation plane; scale bar: 1 mm. (**A'**) Qualitative and quantitative analyses of regeneration efficiency for the different conditions tested. RI: regeneration index; a. u.: arbitrary units. (**B**) Vehicle-control does not affect V_m at either 6 or 24 hpa. (**C**) Vehicle-control does not affect TEP at 6 hpa. (**D**) Vehicle-control does not affect J_I at either 6 or 24 hpa. *n* specimens indicated in brackets.

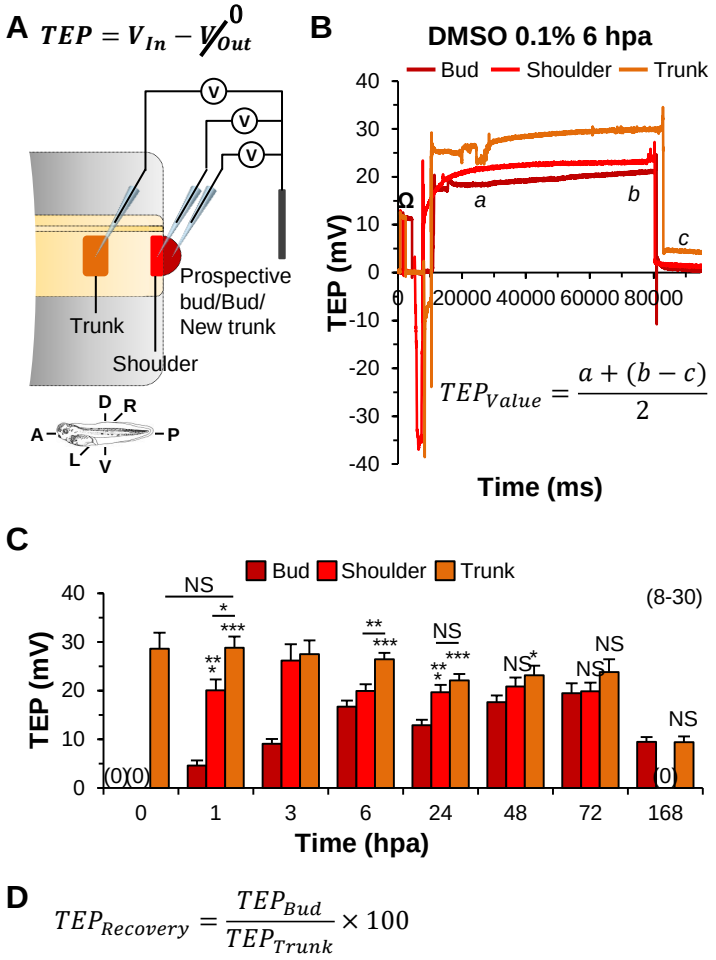

Fig. S2. Spatiotemporal profiles of extracellular bioelectricity during tail regeneration: TEP. (**A**) Lateral view of a schematic tail (at 6 hpa) depicting the experimental design, regions of interest (ROIs) and general equation. Measuring microelectrode (V_{In}) was impaled through the epithelial layers (one ROI at a time) and the circuit was closed by a reference electrode (V_{Out}) in the medium. ROIs were measured at the D/V axis intersection, irrespective of left-right (L/R) axis, as follows: uncut trunk: at half the tail; bud: posterior to amputation plane; shoulder: anterior to amputation plane; and trunk, over intact somites. ROIs are color-coded and also apply to **B** and **C**. Schemes of tails are displayed in the same orientation as the whole organism A/P, D/V and L/R axes (bottom scheme; applies to subsequent figures). (**B**) Representative result and specific equation used to calculate TEP value as a modified mean from raw data. Ω is the electrode resistance, where 10 mV equates to 1 MΩ. Resistance reading prior impalement is a technical control to guarantee that tip was neither broken nor obstructed. TEP was recorded for *ca.* 1 minute and after microelectrode withdrawal potential typically returned to 0 mV. If the reference baseline (*c*) was >±1 and ≤±5 mV, value was subtracted to the TEP recorded as shown in the equation; if >±5 mV, trace was rejected. (**C**) Spatiotemporal profile of TEP during regeneration in vehicle-control (DMSO 0.1%). *n* specimens indicated in brackets. (**D**) Specific equation used to calculate bud TEP recovery as a normalized percentage from TEP data of **C**. TEP recovery profile is shown in Fig. 1B.

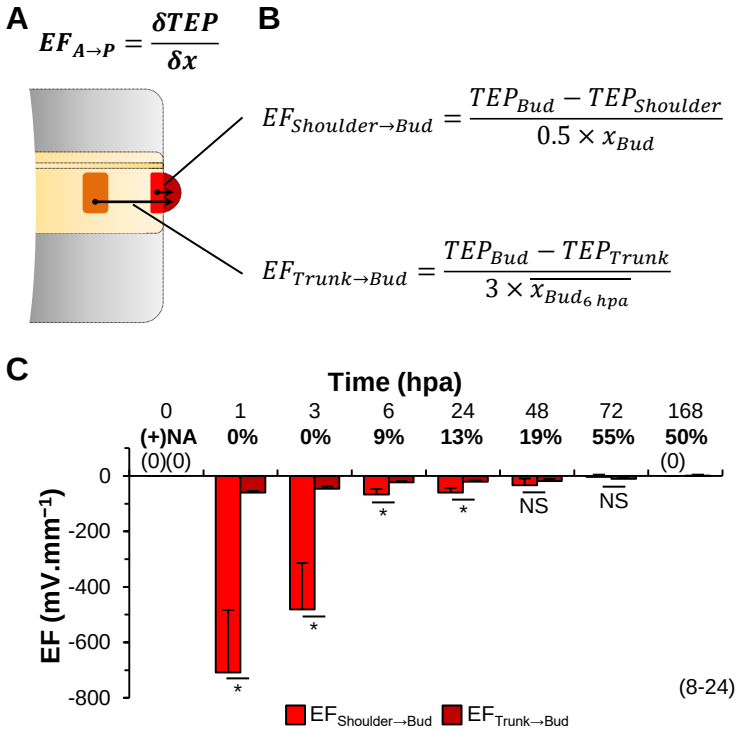

Fig. S3. Spatiotemporal profiles of extracellular bioelectricity during tail regeneration: EF. (**A**) Lateral view of a schematic tail (at 6 hpa) depicting the experimental design, ROIs and general equation. Distances (δx) were obtained from tail photomicrographs (details to follow). ROIs are the same as those shown in Fig. S2A. (**B**) Specific equations used to calculate lateral EF from TEP data of Fig. S2C. Distances (denominators) were challenging to measure because the microelectrode tip was virtually invisible once impaled and because the tail/tadpole commonly moved place due to the microelectrode impalement (inherently mechanical). Thus, even taking consecutive photomicrographs, it was hard to accurately measure the distances between the three ROIs every time impaled. To overcome this, we used the very consistent regeneration bud length at 6 hpa as a relative size reference and then defaulted to measure TEP for bud at its half and for trunk at 2.5× the 6 hpa bud size, starting from the shoulder. Shoulder was therefore at distance 0 mm. In this way, for all tails we just needed to take one photomicrograph of the bud and measure its length for each tadpole. Then we calculated the mean of all 6 hpa buds and fixed that value (0.134±0.009 mm, n=24) for $\overline{x_{Bud_{6\ hpa}}}$. For $EF_{Shoulder\to Bud}$ equation denominator, the bud/new trunk length was always directly measured at all time-points and then halved to represent the distance from shoulder to bud. (**C**) Spatiotemporal profile of lateral EF during regeneration in vehicle-control (DMSO 0.1%). Frequencies of potential/EF reversals (total percentage of TEP_{Trunk}<TEP_{Bud}, hence anode (positive pole) at bud) are given under condition bars for $EF_{Trunk\to Bud}$. Data of $EF_{Trunk\to Bud}$ are the same as those shown in Fig. 1C. NA: not applicable; n specimens indicated in brackets.

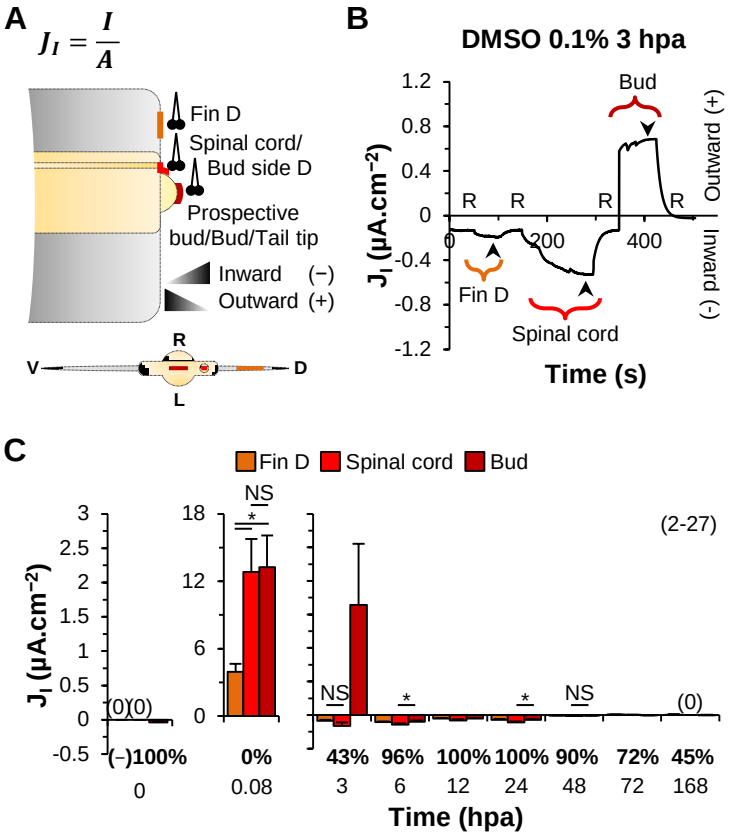

Fig. S4. Spatiotemporal profiles of extracellular bioelectricity during tail regeneration: J_I. (**A**) Lateral view of a schematic tail (at 6 hpa) depicting the experimental design, ROIs and general equation. Probe (~5-10 µm from tail surface) shows the double image of the platinum tip ball (~30 µm diameter) generated by a vibration between 100-200 Hz. By convention, flux of positive charge is used for electric current direction. As in most studies, we used conventional current flow, thus outward current density is defined as net positive charge leaving the tail/regenerate and inward current densities as that entering. Hence, positive values represent net outward current densities and negative values represent net inward current densities (applies to subsequent figures). Bottom: back view schematic detail pinpointing ROIs measured at L/R axis intersection; uncut tail was measured at tail tip. We also measured currents in the muscle V/bud side V and in the fin V. However, because values were non-significant in symmetric D and V positions at 6 and 24 hpa (data not shown), we then measured only the annotated ROIs in the schemes. ROIs are color-coded and apply to **B** and **C**. *I*: electric current; *A*: area. (**B**) Representative result from raw data. J_I was recorded until stable peak was reached (<1 minute). R: reference position measurement (>>1 mm from tail surface); arrowhead: extracted plateau peak value. (**C**) Spatiotemporal profile of J_I during regeneration in vehicle-control (DMSO 0.1%). Frequencies of current reversals (total percentage of inward J_I) are given under condition bars for bud. Data of regeneration bud are the same as those shown in Fig. 1D. *n* specimens indicated in brackets.

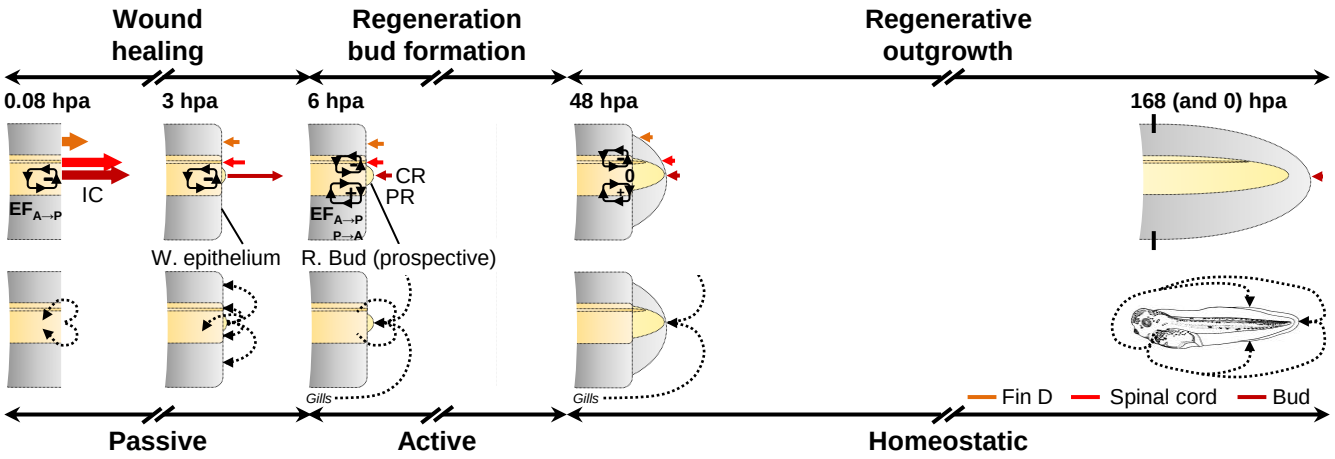

Fig. S5. Spatiotemporal profiles of extracellular bioelectricity during tail regeneration: integration. Schematic representation integrating spatiotemporal bioelectric activities during regeneration of a tadpole amputated at st. 40-41. Electric current (over bottom schemes) and EF (over top schemes) circuits are hypothetical and mainly based on Fig. S2C, S3C, S4C. The whole organism electric circuit – large outward current at gills and small inward currents elsewhere – is based on previous data (Reid *et al*., 2009). Profiles are divided into three phases according to the bioelectric activity: passive, active and homeostatic. ROIs are the same as those shown in Fig. S4A. Colored solid arrows: net outward (left arrow) or inward (right arrow) current density; black solid arrows: simplified electric field lines; black dotted arrows: simplified current field (circuit) lines. Arrows are not at absolute scale, but present the relative spatiotemporal directions and magnitudes of the currents and circuit loops and fields. Key: A: anterior; P: posterior; IC: injury current; CR: current reversal; PR: potential reversal; W. epithelium: wound epithelium; R. bud: regeneration bud. Black solid lines: amputation plane.

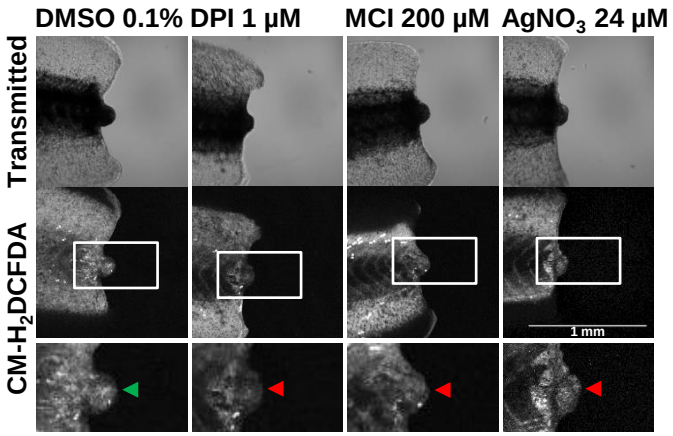

Fig. S6. Redox modulating drugs decrease ROS levels in the bud. Representative tails under transmitted light (top panels) and fluorescence imaging (middle panels) of ROS-sensitive dye CM-H_2DCFDA in vehicle-control (DMSO 0.1%) or pharmacological treatment at 6 hpa. Bottom panels: close up of correspondent rectangles in top panels. Green arrowhead: high ROS levels in the regeneration bud; red arrowhead: low ROS levels in the regeneration bud; scale bar: 1 mm.

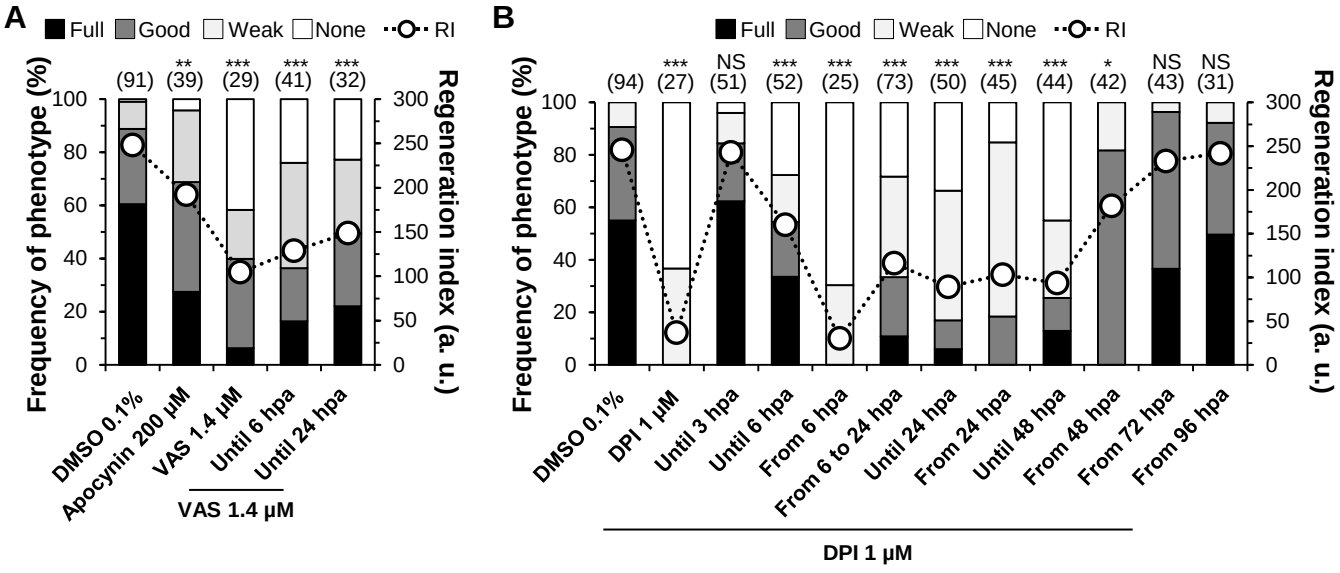

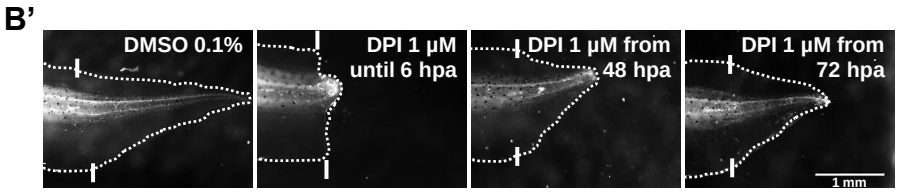

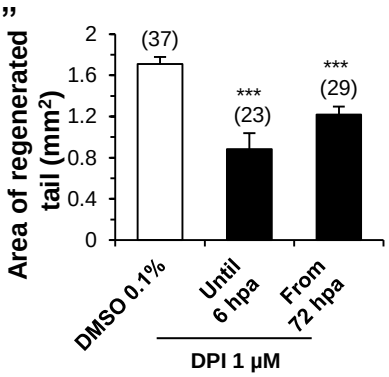

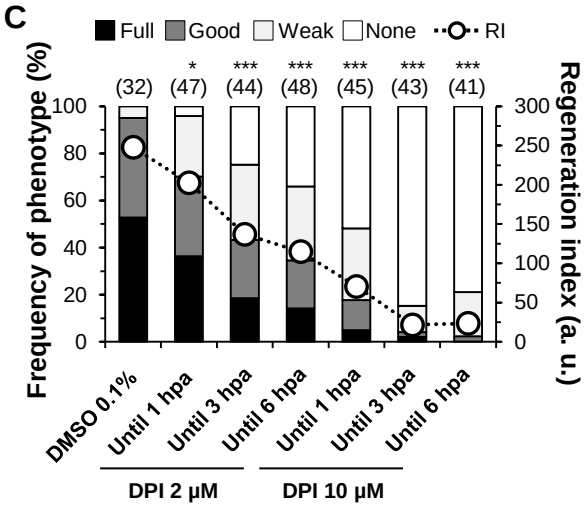

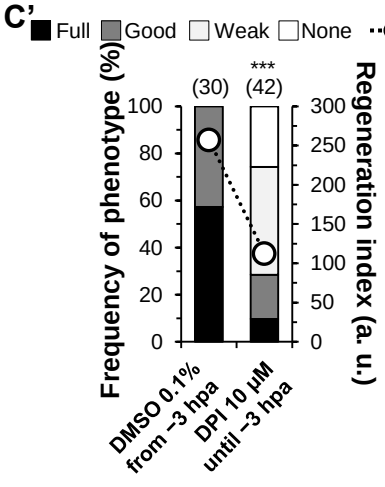

Fig. S7. NADPH oxidase-mediated ROS production is necessary for regeneration in dose- and time-dependent ways. (**A**) Alternative whole family NADPH oxidases inhibitors apocynin and VAS impair regeneration. Short-term exposure (until 6 or 24 hpa) to VAS is enough to impair regeneration. (**B-C'**) Pleiotropic and multi-phase effects of ROS in regeneration. (**B**) Temporal, multi-phase screening of requirement for NADPH oxidase-mediated ROS production during regeneration. ROS are necessary for successful morphogenesis in the first 72 hpa, being independently required for all the three phases of regeneration. (**B',B"**) Thresholds for DPI 1 µM exposure time required to impair regeneration. Until 6 hpa ROS affects global morphogenesis and after 72 hpa, besides no significant effect on morphogenesis, ROS still affect outgrowth (likely through proliferation impairment). (**B'**) Representative 7 dpa tails presenting the thresholds. White solid lines: amputation plane; scale bar: 1 mm. (**B"**) Area of regenerated tail from amputation plane at 7 dpa proving effect of DPI 1 µM in reducing outgrowth if present from 72 hpa. Areas measured from 5 batches of **B**. (**C-C'**) Increasing 2- or 10-fold the dose of DPI reduce even further the required exposure time for significant effect on regeneration from 6 hours to immediately post-amputation, if tadpoles were pre-incubated prior amputation**.** RI: regeneration index; a. u.: arbitrary units. *n* specimens indicated in brackets.

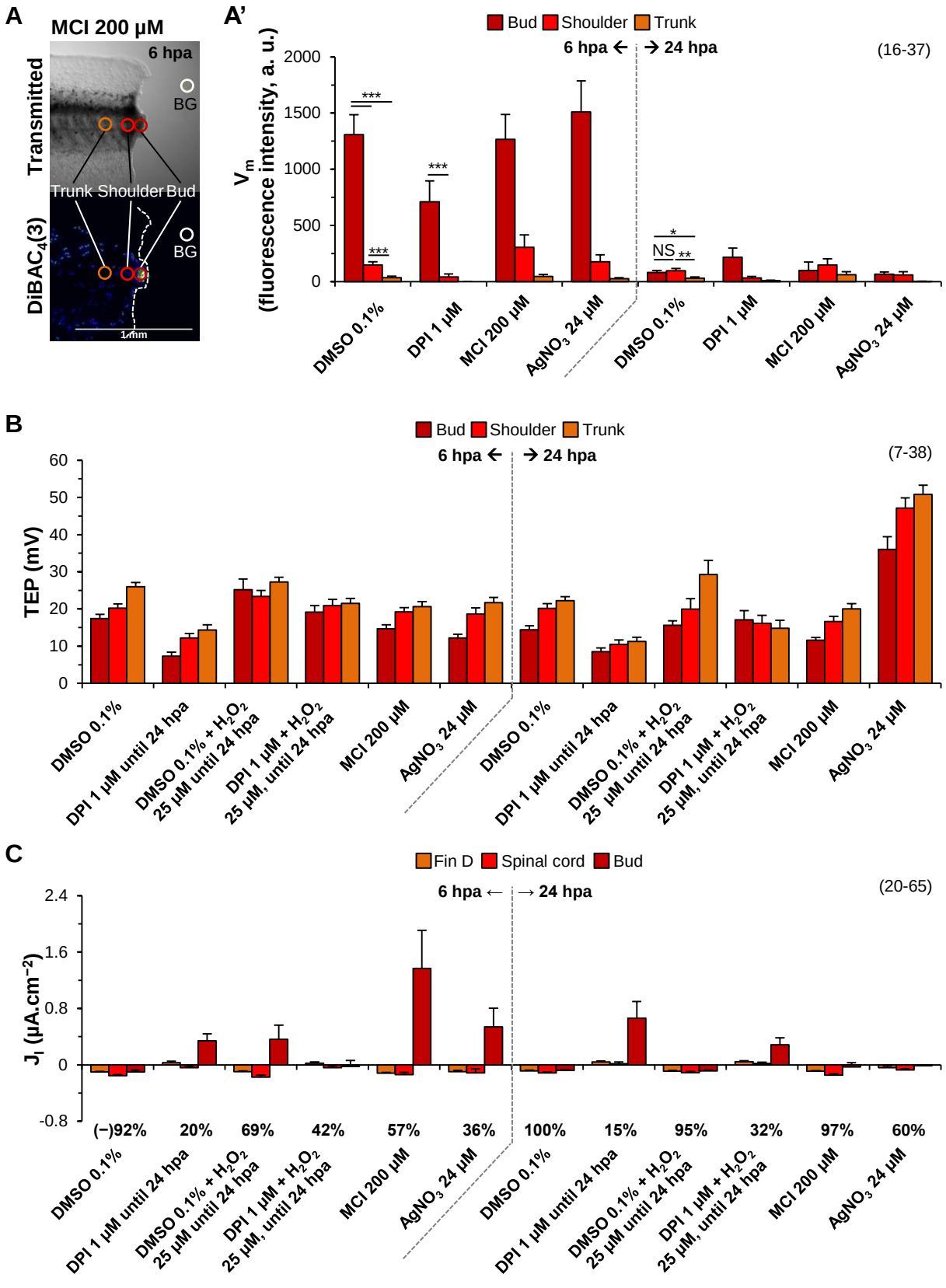

Fig. S8. Electrogenic property of NADPH oxidases is necessary for V_m depolarization and catalytic property for regeneration, TEP increase and J_I reversal, at 6 and 24 hpa in a spatially-dependent way. (**A,A'**) NADPH oxidases activity *per se* depolarizes V_m. (**A**) Representative result at 6 hpa of transmitted light (top panel) and fluorescence imaging (bottom panel) of membrane potential-sensitive dye $DiBAC_4(3)$ depicting the experimental design and circular ROI positions. ROIs were positioned at D/V axis intersection, irrespective of L/R axis, as follow: uncut trunk: at half the tail; bud: posterior to amputation plane; shoulder: anterior to amputation plane; and trunk: over intact somites. Background ROI was placed away from tail. ROIs are color-coded and apply to **A'**. BG: background; scale bar, 1 mm. (**A'**) Spatial profile of relative V_m in different conditions at 6 and 24 hpa. a. u.: arbitrary units. (**B**) Spatial profile of TEP in different conditions at 6 and 24 hpa. Dramatic increase of TEP in $AgNO_3$-treated tails at 24 hpa may be due to silver ions affecting ion translocators (Curran, 1972). (**C**) Spatial profile of J_I in different conditions at 6 and 24 hpa. Frequencies of current reversals (total percentage of inward J_I) are given under condition bars for bud. Data of all regeneration bud at 6 hpa are the same as those shown in Fig. 2B'-D. *n* specimens indicated in brackets.

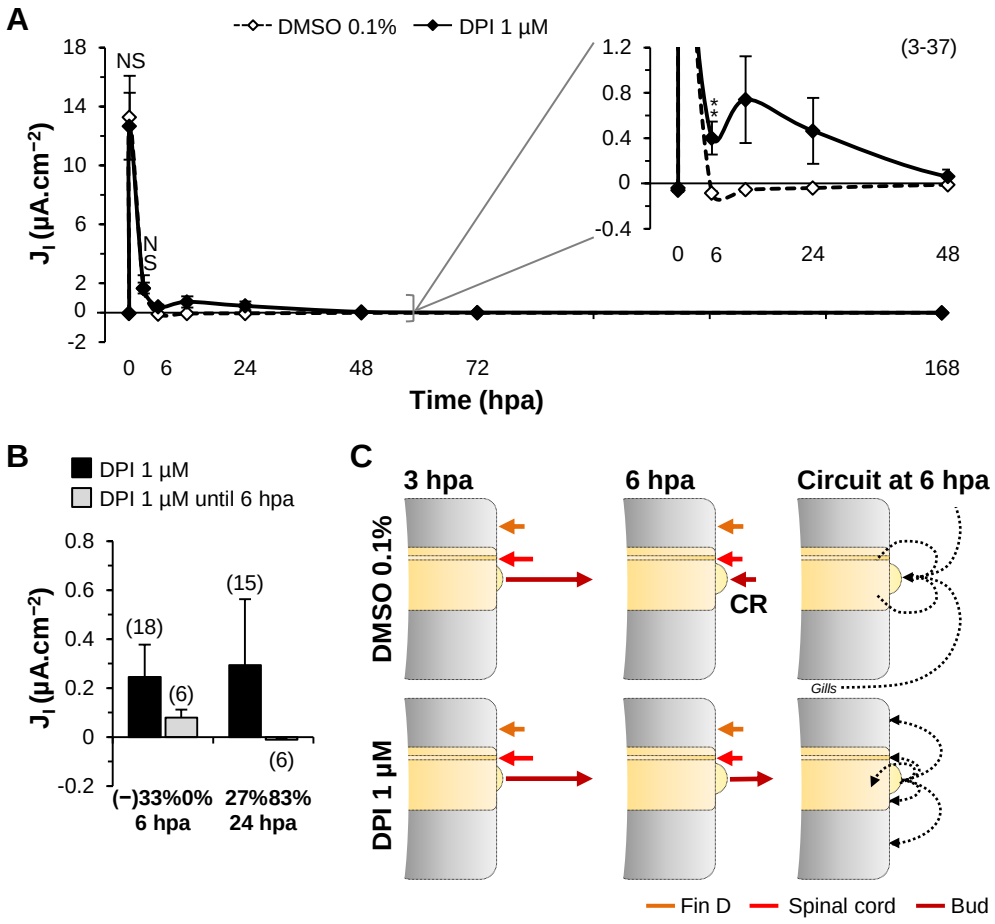

Fig. S9. Inhibition of NADPH oxidase-mediated ROS production prevents current reversal in a reversible way. (**A**) Temporal profile of J_I in the regeneration bud in vehicle-control (DMSO 0.1%) and DPI 1 µM. Data of vehicle-control are the same as those shown in Fig. 1D, being siblings of DPI-treated tadpoles. (**B**) J_I reversal occurs in a delayed way upon wash out of DPI 1 µM. Frequencies of current reversals (total percentage of inward J_I) are given under condition bars. (**C**) Schematic representation integrating spatiotemporal bioelectric activities in early regeneration. J_I reversal does not occur in DPI-treated tails and circuit does not evolve. Colored solid arrows: net outward (left arrow) or inward (right arrow) current density; black dotted arrows: simplified current field (circuit) lines. Arrows are not at absolute scale, but present the relative spatiotemporal directions and magnitudes of the currents and circuit. CR: current reversal. *n* specimens indicated in brackets.

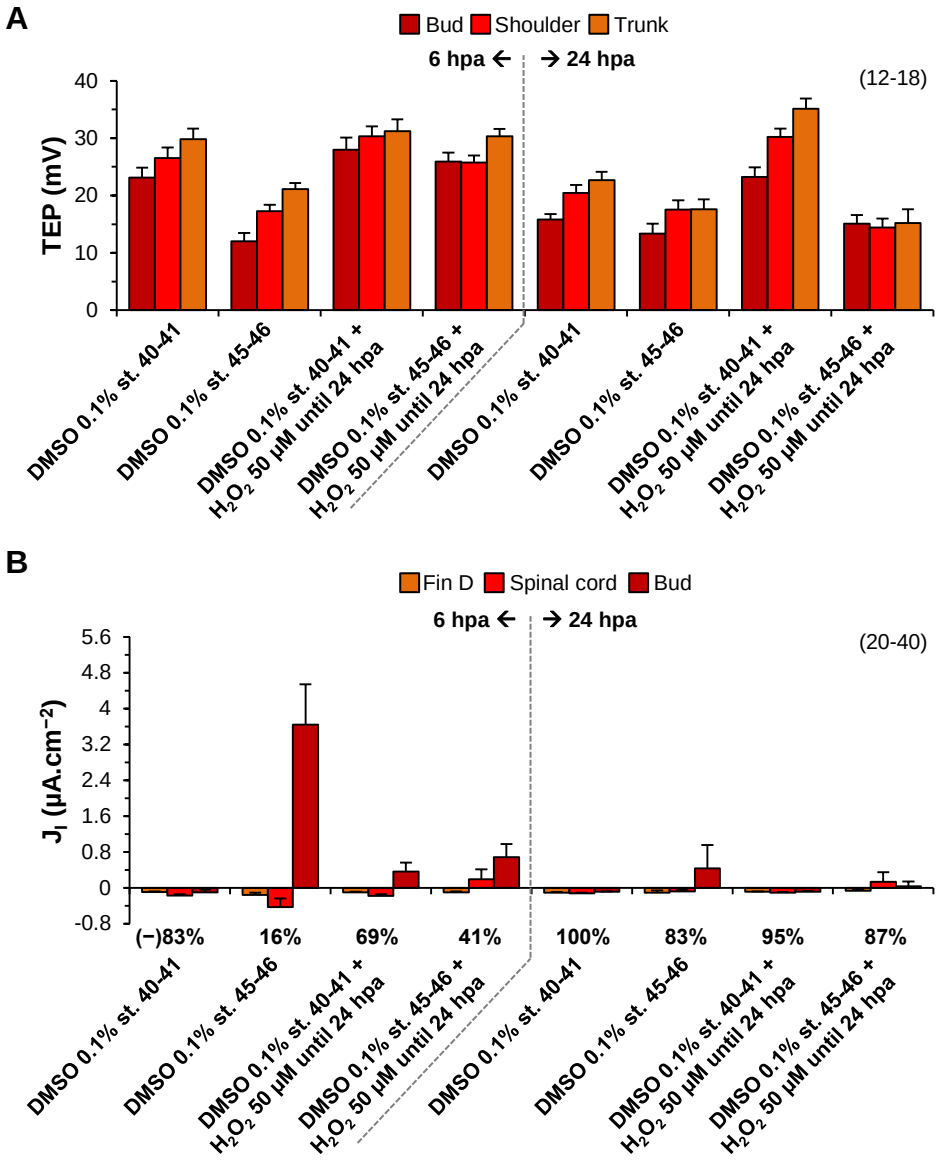

Fig. S10. Exogenous H_2O_2 is sufficient to induce TEP increase and J_I reversal in refractory period at 6 and 24 hpa in a spatially-dependent way. (**A**) Spatial profile of TEP in different conditions at 6 and 24 hpa. (**B**) Spatial profile of J_I in different conditions at 6 and 24 hpa. Frequencies of current reversals (total percentage of inward J_I) are given under condition bars for bud. Data of all regeneration bud at 6 hpa are the same as those shown in Fig. 3B,C. *n* specimens indicated in brackets.

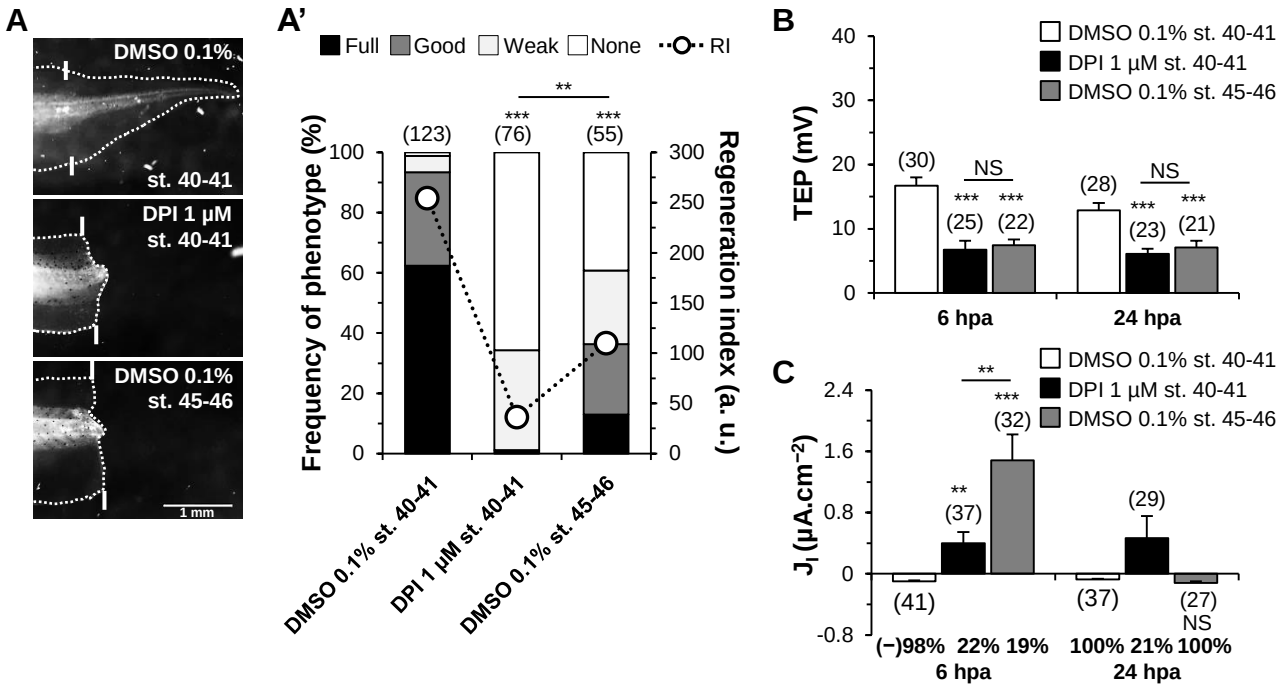

Fig. S11. Inhibited NADPH oxidase-mediated ROS production mimics refractory period regeneration and bioelectric activities. (**A,A'**) Depleted ROS levels mimic refractory period regeneration. (**A**) Representative 7 dpa tails from tadpoles amputated at regenerative (st. 40-41) or refractory period (st. 45-46). Tails were treated with vehicle-control (DMSO 0.1%) or DPI (1 µM). White solid lines: amputation plane; scale bar, 1 mm. (**A'**) Qualitative and quantitative analyses of regeneration efficiency for the different conditions tested. RI: regeneration index; a. u.: arbitrary units. (**B**) Reduced ROS levels mimic refractory period TEP at 6 and 24 hpa. (**C**) Reduced ROS levels mimic refractory period J_I direction at 6 hpa. Frequencies of current reversals (total percentage of inward J_I) are given under condition bars. *n* specimens indicated between brackets.

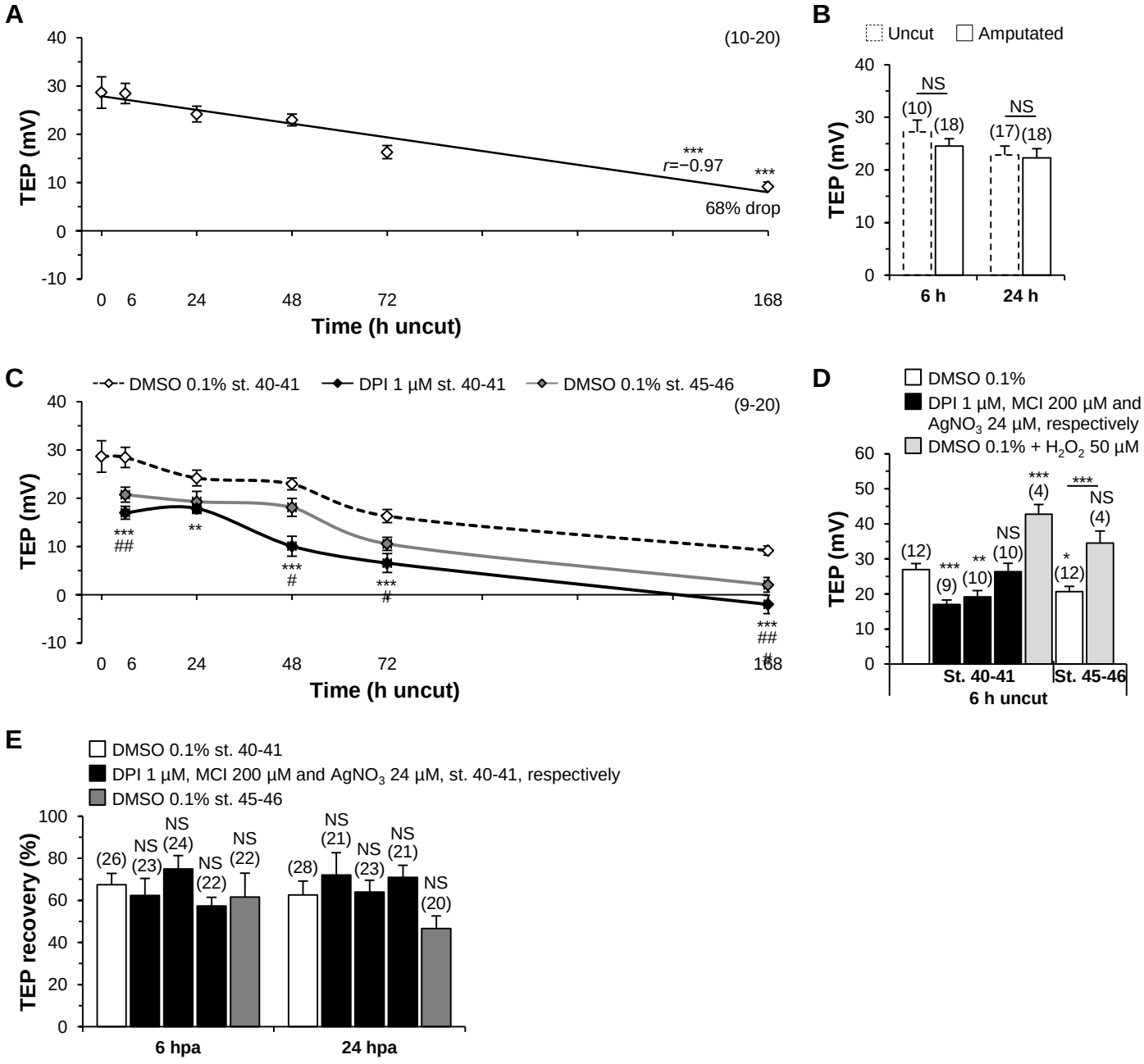

Fig. S12. ROS modulation and amputation in refractory period *per se* affect TEP in a regeneration-unspecific way. (**A**) Temporal profile of TEP during development in vehicle-control (DMSO 0.1%). Uncut trunk TEP is ontogeny-dependent, *i.e.*, inversely proportional to developmental time (r=−0.97, P=0.0009). TEP significantly decreases up to 68% (n=17, P<0.0001) in a linear way (r^2=0.95) as tadpole develops in the same time-window of regeneration (7 days). Solid line: linear regression; r: correlation coefficient. (**B**) Trunk TEP baseline is amputation-independent and regeneration-unspecific in vehicle-control. (**C**) Temporal profile of TEP during development in depleted ROS (DPI 1 µM) and refractory period (vehicle-control) conditions. TEP baseline shifts in the

same way (decreases) as regeneration bud in DPI-treated and refractory period tails. The same shift occurs in MCI-treated tadpoles (temporal profile not plotted for clarity; isolated 6 h uncut time-point in **D**). Depleted ROS levels in uncut tails thus mimic refractory period. Applied H_2O_2 also shifts uncut trunk TEP baseline in the same way (increases) as bud (temporal profile not plotted for clarity; isolated 6 h uncut time-point in **D**). Therefore, TEP variations are potentially systemic, with effects in housekeeping translocators likely regulated by H_2O_2. Data of DMSO 0.1% st. 40-41 are from **A**, being siblings of DPI-treated and refractory period tadpoles. *: *vs.* DPI 1 µM st. 40-41; $^{\#}$: *vs.* DMSO 0.1% st. 45-46. (**D**) Representative uncut time-point (6 h). Depleted ROS levels and amputation in refractory period shift TEP baseline the same way as bud subjected to the same conditions. Most data of DMSO 0.1% st. 40-41 and st. 45-46, and all data of DPI 1 µM are from **C**. (**E**) Depleted ROS levels and amputation in refractory period do not affect TEP recovery. This is the consequence of a similar shift in direction and magnitude of bud and trunk TEP in these conditions. *n* specimens indicated in brackets.

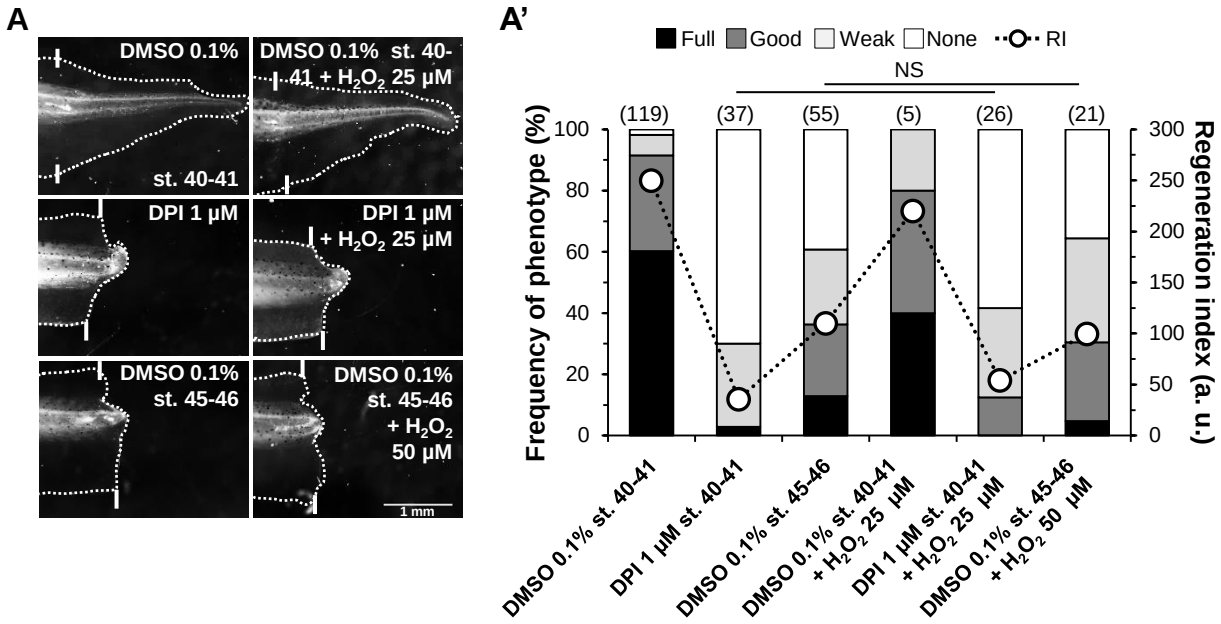

Fig. S13. Exogenous H_2O_2 loses ability to rescue and induce regeneration when present throughout regeneration. (**A**) Representative 7 dpa tails amputated from tadpoles during the regenerative (st. 40-41) or refractory (st. 45-46) periods. Tails were treated with vehicle-control (DMSO 0.1%) or pharmacological treatment. White solid lines: amputation plane; scale bar: 1 mm. (**A'**) Qualitative and quantitative analyses of regeneration efficiency for the different conditions tested. RI: regeneration index; a. u.: arbitrary units. *n* specimens indicated in brackets.

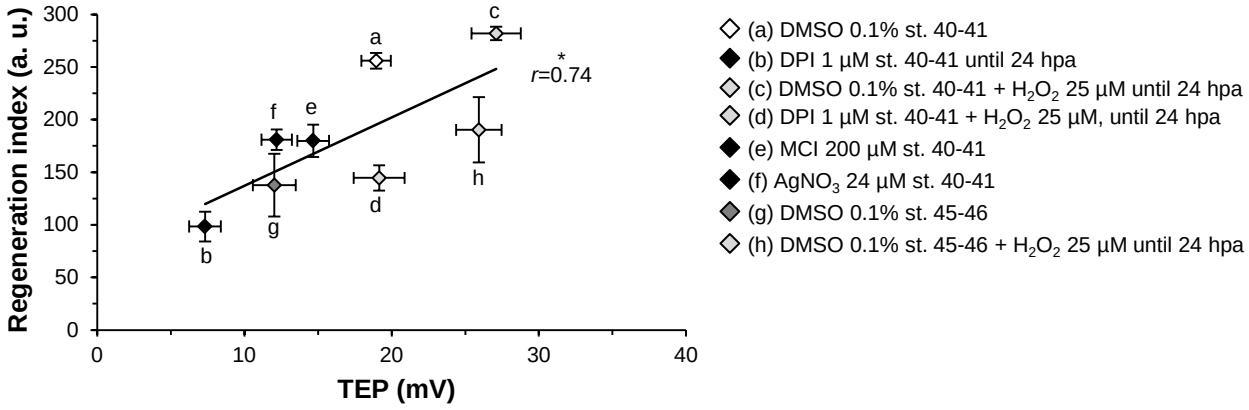

Fig. S14. Regeneration efficiency is directly proportional to TEP magnitude. Compilation of the different conditions tested. Data of regeneration index are from Fig. 2A', 3A' and data of TEP magnitude are from Fig. 2C, 3B. Due to multiple impalements for TEP measurements, tadpoles were not followed for regeneration efficiency analysis. Thus, part of the data crossed is not matched siblings. Solid line: linear regression (r^2=0.55); r: correlation coefficient (P=0.036).

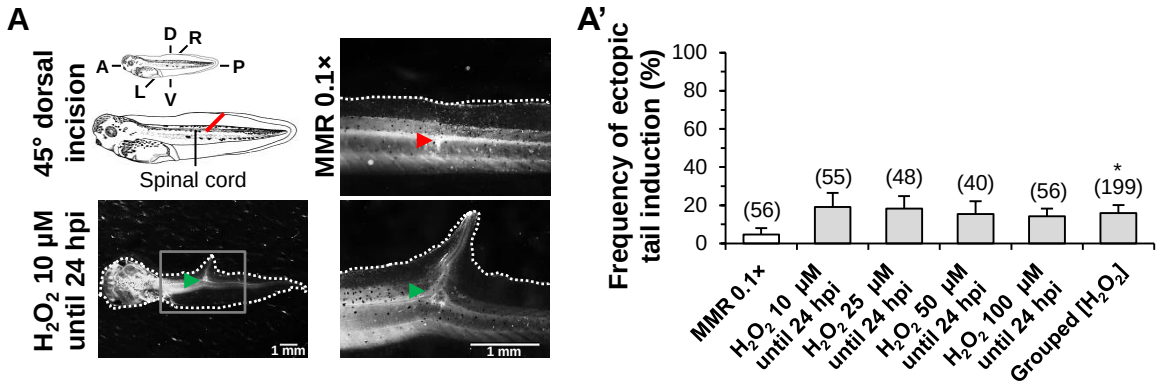

Fig. S15. Exogenous H_2O_2 induces ectopic (abnormal or complete) tails upon dorsal incision severing the spinal cord. (**A**) Top right panel: schematic tadpole at st. 40-41 depicting the experimental design of the angled incision. Bottom right and top and bottom left panels: representative 7 days post-incision tails in control (MMR 0.1×) and supplemented with a representative dose of H_2O_2 until 24 hours post-incision (hpi). Bottom left panel: close up of rectangle in bottom right panel. Red solid line: incision plane; red arrowhead: incision healed without ectopic tail induction; green arrowhead: incision endpoint with ectopic tail induction. Note that ectopic tail presents recognizable structure (with trunk and fins) and pigmentation (also has blood flow). Scale bar: 1 mm. (**A'**) Ectopic tail induction is dose-independent. This was the case at least for short-term exposure (24 hours) and relatively low doses (µM range) of H_2O_2. Frequency of abnormal or complete ectopic tails slightly augmented in *ca.* 10-15% above the *ca.* 5% baseline frequency of control. Exogenous H_2O_2 (tested 50 and 200 µM) loses ability to induce ectopic tails when present throughout 7 days (data not shown). *n* specimens indicated in brackets.

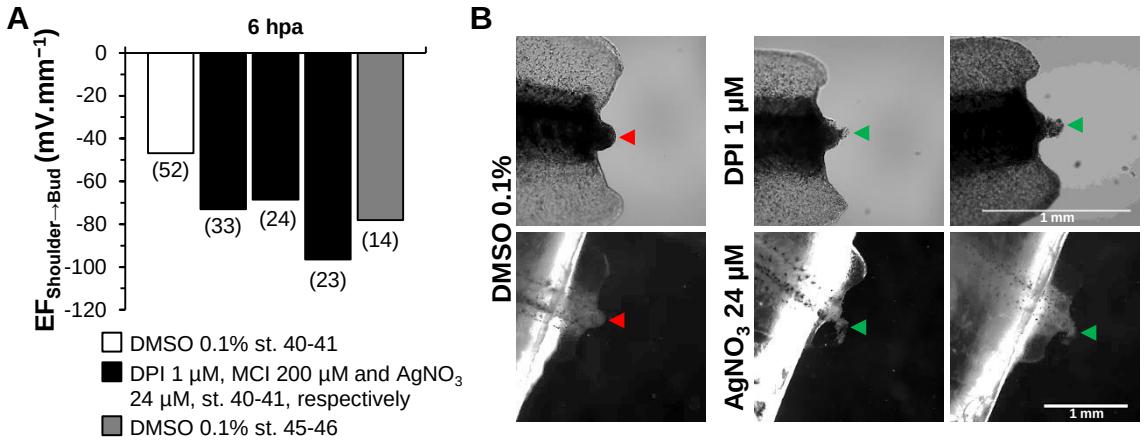

Fig. S16. ROS modulation mimics the stronger EF of refractory period that might be a guiding cue for possible epithelial cells overmigration. (**A**) Depleted ROS levels mimic refractory period lateral, shoulder to bud, EF at 6 hpa. Mean EF are calculated from mean TEP data of Fig. S8B, S10A. (**B**) Representative tail phenotypes in vehicle-control (DMSO 0.1%) at st. 40-41 and pharmacological treatment at 6 hpa. Circumstantial evidence of 'cloud' phenotype may indicate cell overmigration in ROS-modulated tails, usually not present in vehicle-control tails. Red arrowhead: cloud absence; green arrowhead: cloud presence; top panels: transmitted light; bottom panels: bright field; scale bars: 1 mm. *n* specimens indicated in brackets.

Supplementary Materials and Methods

Animals and surgery

Xenopus laevis tadpoles were incubated at temperatures between 13 to 33 °C until the desired stages, st. 40-41 (regenerative) or st. 45-46 (refractory period), for amputation were reached.

Tadpoles equilibrated to room temperature were immobilized in myosin inhibitor *N*-benzyl-p-toluene sulfonamide 50 µM (BTS; Tocris Bioscience, cat. no. 1870) up to 5 minutes and transferred to the experimental condition still supplemented with BTS. Under a dissecting microscope, half of the tail was quickly amputated with a scalpel (blade no. 10; Feather Safety Razor) (Fig. 1A).

After experiments, tadpoles were euthanized in anesthesia (tricaine, MS-222; Sigma-Aldrich, cat. no. E10521; or Western Chemical) overdose.

Tail regeneration assay

Typically, 8-10 tadpoles per well of 6 well plates were followed at room temperature at a density of ~1 tadpole.ml^{-1}. Experimental conditions were refreshed daily and tadpoles were not fed during regeneration. Under a microscope (Zeiss Lumar V12) with attached monochromatic CCD camera (Zeiss AxioCam MRm), tail photomicrographs at 7 dpa were acquired using AxioVision software (Zeiss).

Regeneration efficiency per well was scored using the composite regeneration index introduced and described previously (Adams *et al.*, 2007; Tseng *et al.*, 2010). Briefly, regeneration outcome was characterized as full, good, weak and none phenotypes and then RI was calculated using Excel (Microsoft). RI ranges, in arbitrary units, from 0 (all none) to 300 (all full). Against control tails, RIs ≥250 and ≤100 represent unimpaired and highly impaired regeneration, respectively. Unlike length or area of regenerated tail, RI gives a measure of the morphogenetic quality, combining axes outgrowth and patterning.

In a single case we measured area of regenerated tail to specifically analyze outgrowth. Area was measured using ImageJ (http://rsbweb.nih.gov/ij/).

Data were treated using Excel.

Ectopic tail induction

Immobilized tadpoles were mounted on filter paper (Whatman, cat. no. 1001-090) wetted with the experimental condition. Using a scalpel or knife (Premier Edge Stab 15°; Oasis Medical), a 45° dorsal incision severing down to the spinal cord (inclusive) was made at half the tail (Fig. S15A) (Sugiura *et al.*, 2009). Tadpoles were followed and photomicrographed as the amputated tadpoles.

Frequency of abnormal or complete ectopic tails per well was calculated using Excel.

Pharmacological modulations

Tadpoles treated with light-sensitive drugs ($AgNO_3$, H_2O_2 and tricaine) were followed in the dark.

Extensive dose-exposure screenings made for applied drugs were designed so final vehicle DMSO would be typically ≤0.1%. Mostly, selected dose and exposure presented no toxicity and normal development while affecting regeneration. However, in long-term exposure or high dose of DPI, tadpoles were smaller and less pigmented than vehicle-control. MCI-treated tadpoles were also smaller and presented some defects in the intact trunk (some curvature). A single toxic treatment was used; the

combination of H_2O_2 and tricaine in tadpoles amputated at st. 45-46 (~60% died). Intriguingly, no death occurred at st. 40-41, suggesting stage-specific toxicity. Wells in which ≥3 tadpoles survived were accepted.

For every drug treatment, matched sibling controls were performed. To allow ready cross comparisons, the basic control used was the vehicle-control DMSO 0.1% (non-significant effect on readouts; Fig. S1). Thus, when indicated, drugs were washed out to DMSO 0.1%, except in the ectopic tail induction assays (to MMR 0.1× instead).

ROS and V_m fluorescence imaging

ROS and V_m were imaged using the vital dyes chloromethyl derivative of 2',7'-dichlorofluorescein (CM-H_2DCFDA; Molecular Probes; cat no. C6827) and bis-(1,3-dibutylbarbituric acid)trimethine oxonol ($DiBAC_4(3)$; Molecular Probes; cat no. B438), respectively. CM-H_2DCFDA was prepared prior to use in anhydrous DMSO (Sigma-Aldrich, cat. no. 276855) at 10 mM and $DiBAC_4(3)$ was stocked at 2 mM in DMSO at −20 °C. Dyes were freshly reconstituted in the experimental conditions.

Tadpoles amputated at st. 40-41 were incubated at room temperature in the dark in CM-H_2DCFDA 10 µM up to 2 hours, or in $DiBAC_4(3)$ 2 µM for ~30 minutes. Individually immobilized tadpoles placed in a microscope lamina with wells and covered with a lamella (thickness no. 1.5) were imaged using UPLSAPO 10x/NA 0.40 or UPlanFl 10x/NA 0.30 objectives (Olympus) mounted in inverted confocal microscopes (Olympus FV1000 or FV300 confocal systems). CM-H_2DCFDA was washed out during immobilization. Excitation wavelength was 488 nm for both dyes.

Maximum projections of acquired *z* plan scans were pseudo-colored with the look-up table gray or thal. In V_m analysis, circular regions of interest (ROIs) – uncut tail trunk and amputated tail bud, shoulder and trunk – were positioned as previously detailed (Adams *et al.*, 2007) (Fig. S8A). For each ROI, mean pixel intensity was measured and background was subtracted.

V_m was scattered in uncut trunk of vehicle-control (as reported (Adams *et al.*, 2007)) and drug treatments (data not shown). Thus, no normalization of amputated tails was performed. Therefore, the total range of pixel intensities (0 to 4095) was considered as the semi-quantitative, relative value of V_m.

The imaging settings were kept constant across experiments. Technical (for electronic noise), negative (for autofluorescence and wavelength selectivity) and positive (high H_2O_2 or K^+) controls gave conservative expected results.

Data were acquired and extracted using FluoView (Olympus) and treated using ImageJ and Excel.

Glass microelectrode measurement

Microelectrodes (1-2 µm tip diameter; NaCl 3 M electrolyte) had resistances of ~1-2 MΩ. Immobilized tadpoles were positioned in the non-conductive measuring chamber and electrode potential offset to 0 mV prior to impalement. TEP was recorded for *ca.* 1 minute in the ROIs (same as for V_m) and times indicated (Fig. S2A,B).

Tadpole regeneration was not followed in subsequent days due to multiple impalements. Measurements occurred at room temperature. Tadpoles were visualized under a microscope (same as for photomicrographs) within a Faraday cage on an anti-vibration table.

To efficiently discriminate developmental (McCaig and Robinson, 1982) (Fig. S12A) from

regenerative TEP variations we normalized bud TEP against trunk TEP. This is correct because trunk TEP was regeneration-unspecific (Fig. S12B). TEP recovery was thus calculated as a normalized percentage (Fig. S2D).

Lateral EF were calculated from TEP data (Fig. S3A,B).

Data were acquired (sampling of 100 Hz) and extracted using pClamp 10 (Molecular Devices) and treated using Excel.

Vibrating probe measurement

The probes, platinum-electroplated at the tip (~30 µm ball diameter), vibrated at a frequency between 100-200 Hz. Prior to measurements, probe was calibrated in experimental conditions by an applied J_I of 1.5 µA.cm^{-2}.

Under a dissecting microscope, immobilized tadpoles were positioned in the non-conductive measuring chamber. Plane of probe vibration was perpendicular to the tail surface at a distance of ~5-10 µm. J_I was recorded until plateau peak reached (<1 minute) in the ROIs – uncut tail tip and amputated tail fin, spinal cord and bud – and times indicated. Reference values were recorded with probe away from tail (>>1 mm) (Fig. S4A,B).

Tadpole regeneration was followed. Measurements occurred at room temperature. During calibrations and measurements a Faraday 'wall' (grounded aluminum-wrapped cardboard) covered the microscope.

Data were acquired and extracted using WinWCP V4 (Strathclyde Electrophysiology Software) and treated using Excel.

Statistical analysis

Regeneration efficiencies between two groups were compared using raw observations (counts) from full and none outcomes. These extreme phenotypes are more likely to increase the sensitivity of the analysis, performed with the Fisher's exact test. However, if assumptions of the test were not fulfilled or if discrete observations were small sized or very unbalanced, we occasionally carried the analysis using combined raw observations from full+good and weak+none outcomes. Usually, *P* values were similar using either raw data.

For the unpaired Student's *t* test, pre-tests were performed for normality and equal variances assumptions of parametric tests. Normality was tested with Kolmogorov-Smirnov, Shapiro-Wilk and/or D'Agostino and Pearson, and variances with *F* or Bartlett's pre-tests. Assumptions were typically verified; if not, sample sizes (*n*, biological replicates) were large to minimize normality influence and Welch's correction was applied when unequal variances.

Two-tailed *P* value was used as default. However, when we expected (by previous data) a decrease or increase in the readout, one-tailed *P* value was occasionally used (seldom cases within Mann-Whitney *U* test).

Supplementary References

Adams, D. S., Masi, A. and Levin, M. (2007). H^+ pump-dependent changes in membrane voltage are an early mechanism necessary and sufficient to induce Xenopus tail regeneration. *Development* **134**, 1323–35.

Curran, P. F. (1972). Effect of silver ion on permeability properties of frog skin. *Biochim. Biophys. Acta* **288**, 90–97.

Reid, B., Song, B. and Zhao, M. (2009). Electric currents in Xenopus tadpole tail regeneration. *Dev. Biol.* **335**, 198–207.

Sugiura, T., Tazaki, A., Ueno, N., Watanabe, K. and Mochii, M. (2009). Xenopus Wnt-5a induces an ectopic larval tail at injured site, suggesting a crucial role for noncanonical Wnt signal in tail regeneration. *Mech. Dev.* **126**, 56–67.

Tseng, A.-S., Beane, W. S., Lemire, J. M., Masi, A. and Levin, M. (2010). Induction of vertebrate regeneration by a transient sodium current. *J. Neurosci.* **30**, 13192–200.